CellPress

Neuron
Article

Miniature Neurotransmission Regulates *Drosophila* Synaptic Structural Maturation

Ben Jiwon Choi,[1,2,3] Wendy L. Imlach,[1,2,4] Wei Jiao,[1,2,4] Verena Wolfram,[5] Ying Wu,[6] Mark Grbic,[1,2] Carolina Cela,[1,2] Richard A. Baines,[5] Michael N. Nitabach,[6] and Brian D. McCabe[1,2,4,*]

[1]Department of Pathology and Cell Biology
[2]Center for Motor Neuron Biology and Disease
[3]Department of Physiology and Cellular Biophysics
[4]Department of Neuroscience
College of Physicians and Surgeons, Columbia University, New York, NY 10032, USA
[5]Faculty of Life Sciences, University of Manchester, Manchester M13 9PL, UK
[6]Department of Cellular and Molecular Physiology, Department of Genetics, Program in Cellular Neuroscience, Neurodegeneration and Repair, Yale School of Medicine, New Haven, CT 06520, USA
*Correspondence: brian@mccabelab.org
http://dx.doi.org/10.1016/j.neuron.2014.03.012

SUMMARY

Miniature neurotransmission is the transsynaptic process where single synaptic vesicles spontaneously released from presynaptic neurons induce miniature postsynaptic potentials. Since their discovery over 60 years ago, miniature events have been found at every chemical synapse studied. However, the in vivo necessity for these small-amplitude events has remained enigmatic. Here, we show that miniature neurotransmission is required for the normal structural maturation of *Drosophila* glutamatergic synapses in a developmental role that is not shared by evoked neurotransmission. Conversely, we find that increasing miniature events is sufficient to induce synaptic terminal growth. We show that miniature neurotransmission acts locally at terminals to regulate synapse maturation via a Trio guanine nucleotide exchange factor (GEF) and Rac1 GTPase molecular signaling pathway. Our results establish that miniature neurotransmission, a universal but often-overlooked feature of synapses, has unique and essential functions in vivo.

INTRODUCTION

Two forms of neurotransmission (NT) occur at fast chemical synapses: evoked NT and the much less studied process of miniature NT. During evoked NT, action potentials trigger the release of multiple synaptic vesicles inducing the synchronous activation of many postsynaptic receptors, thereby allowing information to be transmitted across the synaptic cleft. Evoked NT is absolutely essential to brain function and is considered to be the primary carrier for neurochemical communication between neurons. The second form, miniature NT, often called "minis," occurs via the spontaneous release of single synaptic vesicles from presynaptic neurons activating a small number of postsynaptic receptors. Miniature NT is a general property of every fast chemical synapse studied since their discovery by Katz (Fatt and Katz, 1952). However, in contrast to evoked neurotransmission, the in vivo necessity for miniature events has remained a conundrum and they have been often dismissed as a stochastic byproduct of evoked NT (Otsu and Murphy, 2003; Ramirez and Kavalali, 2011; Sutton and Schuman, 2009; Zucker, 2005).

Recent studies, however, have begun to question the notion that miniature events are simply superfluous "noise" derived from the process of evoked NT. First, a number of synaptic vesicle fusion molecules, such as vSNAREs, that are necessary for evoked NT are not essential for miniature NT and vice versa (Kavalali and Monteggia, 2012). Second, specialized synaptic Ca^{2+}-sensing molecules can regulate the frequency of miniature events independently of evoked NT (Walter et al., 2011). Third, some evidence suggests that the synaptic vesicle pools that mediate miniature NT and evoked NT may be distinct, though this remains the subject of active debate (Ramirez and Kavalali, 2011). Fourth, though most active zones at *Drosophila* synapses have both forms of NT, some have recently been shown to produce exclusively miniature or evoked events (Melom et al., 2013; Peled et al., 2014). These studies suggest that miniature events have some properties that are different from evoked NT, prompting the hypothesis that minis could have unique functions at the synapse. Consistent with this idea, in cultured mammalian neurons, miniature NT has been found to influence synaptic scaling, stabilize spine structure, change the activity of postsynaptic kinases, and affect local protein synthesis (Otsu and Murphy, 2003; Sutton and Schuman, 2009; Turrigiano, 2012). However, as of yet, an in vivo function for miniature neurotransmission has not been demonstrated.

One in vivo process that can be disrupted by the depletion of both evoked and miniature NT is synaptic structural development. In mammals, the absence of vesicular NT does not appear to disrupt initial pre- and postsynaptic assembly (Verhage et al., 2000). Nonetheless, when both forms of NT are depleted at neuromuscular synapses, subsequent aspects of synaptic structural development and maturation are perturbed (Kummer

et al., 2006; Witzemann et al., 2013). However, the individual contribution of evoked or miniature neurotransmission to these phenotypes was not dissected in these studies.

A tractable model to investigate synaptic structural development is *Drosophila* glutamatergic larval neuromuscular junction (NMJ) synapses (Collins and DiAntonio, 2007). Like synapses in other systems, *Drosophila* terminals undergo a growth and development phase subsequent to initial synaptic assembly. This process involves a 10-fold expansion of the synaptic terminal area through the iterative addition and enlargement of synaptic varicosities or boutons over 4 days of larval development (Schuster et al., 1996). Like mammalian synapses, the initial assembly of *Drosophila* terminals is not perturbed when both evoked and miniature neurotransmission are abolished (Daniels et al., 2006); however, the effect of a similar depletion on subsequent phases of synaptic development has not been described.

Here, we have investigated the necessity for evoked and miniature neurotransmission during *Drosophila* larval synaptic growth. We found that inhibition of both forms of NT caused characteristic defects in terminal morphology, bouton growth, and ultrastructure. Surprisingly, by manipulating each form of NT independently, we found these defects were caused by the specific loss of miniature NT and not evoked NT. Moreover, we found that increasing miniature NT could promote synaptic growth. We show that miniature NT regulates local synaptic terminal growth by activating a Trio guanine nucleotide exchange factor (GEF), Rac1 GTPase signaling pathway in presynaptic neurons. Our results establish that miniature neurotransmission, an often-overlooked universal feature of all chemical synapses, has a unique and essential role during synaptic development in vivo.

RESULTS

Neurotransmission Is Required for *Drosophila* Larval Synaptic Terminal Development

To determine if neurotransmission is necessary for *Drosophila* larval NMJ synapse development, we sought to inhibit synaptic transmission without perturbing other cellular processes. Vesicular glutamate transporters (Vgluts) are required for the uptake of glutamate into synaptic vesicles (Daniels et al., 2006). *Drosophila* has a single *vglut* gene that completely abolishes all NT at glutamatergic NMJ terminals when eliminated. Importantly, removal of Vglut does not impede either exo/endocytosis (Daniels et al., 2006), which can disrupt synaptic development independently of effects on NT (Dickman et al., 2006). *vglut* null mutants die as embryos, but formation of their synaptic terminals appears normal (Daniels et al., 2006). In order to strongly deplete NT during larval stages (Figure 1H), we combined hypomorphic *vglut* mutants (Daniels et al., 2006; Mahr and Aberle, 2006) with transgenic Vglut-RNAi expressed in motor neurons (MNs) to generate $vglut^{MN}$. In this mutant combination, the amplitude of evoked excitatory postsynaptic potentials (eEPSPs) was reduced by 66% ($p < 0.001$) compared to controls (Figures 1A and 1B; Figure S1A available online). To determine the total amount of evoked NT, we measured the eEPSP integral (Stuart and Sakmann, 1995) (normalized area under the eEPSP above the baseline resting membrane potential [RMP]) (Figure 1E). We found that $vglut^{MN}$ had a 61% ($p < 0.001$) decrease in the eEPSP integral compared to controls (Figure 1F). We also measured miniature excitatory postsynaptic potential (mEPSP) frequency, amplitude, and the mEPSP integral (normalized average area under the mEPSP above the baseline RMP) (Figure 1E). In $vglut^{MN}$ mutants, we found an 89% reduction ($p < 0.001$) in mEPSP frequency (Figures 1B and S1B) but no change in mEPSP amplitude (Figures 1B and S1C), consistent with other *vglut* alleles (Daniels et al., 2006), leading to an 88% ($p < 0.001$) reduction in the mEPSP integral compared to controls (Figure 1G). Thus, in $vglut^{MN}$ mutants, both evoked and miniature NT was inhibited.

When we examined the terminals of $vglut^{MN}$ mutants at the third-instar larval stage (Figure 1H), we found severe morphological defects compared to controls. $vglut^{MN}$ mutants had reduced synaptic terminal area (Figures 1I, 1J, and 1O), but the most striking change we observed was an alteration of individual synaptic bouton sizes (Figures 1K and 1L). In wild-type third-instar larvae, less than 10% of all synaptic boutons are smaller than 2 μm^2, while the majority of boutons are larger than this (Figure S1D). In $vglut^{MN}$ mutants, we observed a dramatic increase in the proportion of boutons smaller than 2 μm^2 (small boutons), while the number of synaptic boutons larger than this (typical boutons) in addition to the total number of boutons was reduced compared to controls (Figure 1P; Table S1). To quantify this shift of bouton sizes, we calculated the ratio of small to typical boutons (bouton size index) and found a 366% ($p < 0.001$) increase in $vglut^{MN}$ mutants compared to controls (Figure 1Q). These phenotypes were observed with multiple *vglut* RNAi lines or hypomorphic *vglut* mutants and could be rescued by transgenic Vglut (Figures S1E–S1H). Similar to typical synaptic boutons, the small boutons in $vglut^{MN}$ mutants had correctly localized markers for active zones, periactive zones, synaptic vesicles, postsynaptic membranes, and postsynaptic receptor fields (Figure S2A). Therefore, *vglut* mutants have synapses with reduced terminal area concomitant with a disproportionally large amount of small synaptic boutons. This result established that even though synaptic transmission is not required for initial embryonic synapse assembly in *Drosophila* (Daniels et al., 2006), it is necessary for the subsequent phase of synaptic terminal growth.

Evoked Neurotransmission Is Not Necessary for Normal Synaptic Terminal Development

In $vglut^{MN}$ mutants, both evoked and miniature forms of neurotransmission are inhibited. Because the majority of NT at *Drosophila* NMJ terminals is via evoked release (Kurdyak et al., 1994), we next used genetically encoded peptide toxins to specifically block this form of NT and dissect its contribution to synapse development. Transgenic tetanus toxin light chain (UAS-TeTxLC) cleaves the vSNARE n-Synaptobrevin, which is essential for evoked, but not miniature, synaptic vesicle release (Sweeney et al., 1995). Expression of TeTxLC in a subset of MNs eliminated the ability of these NMJ terminals to produce evoked release when the axon was stimulated (Figures 1C, 1F, and S2B). In contrast, miniature NT was unaffected (Figures 1C, 1G, S2C, and S2D). As a second independent method of inhibiting evoked

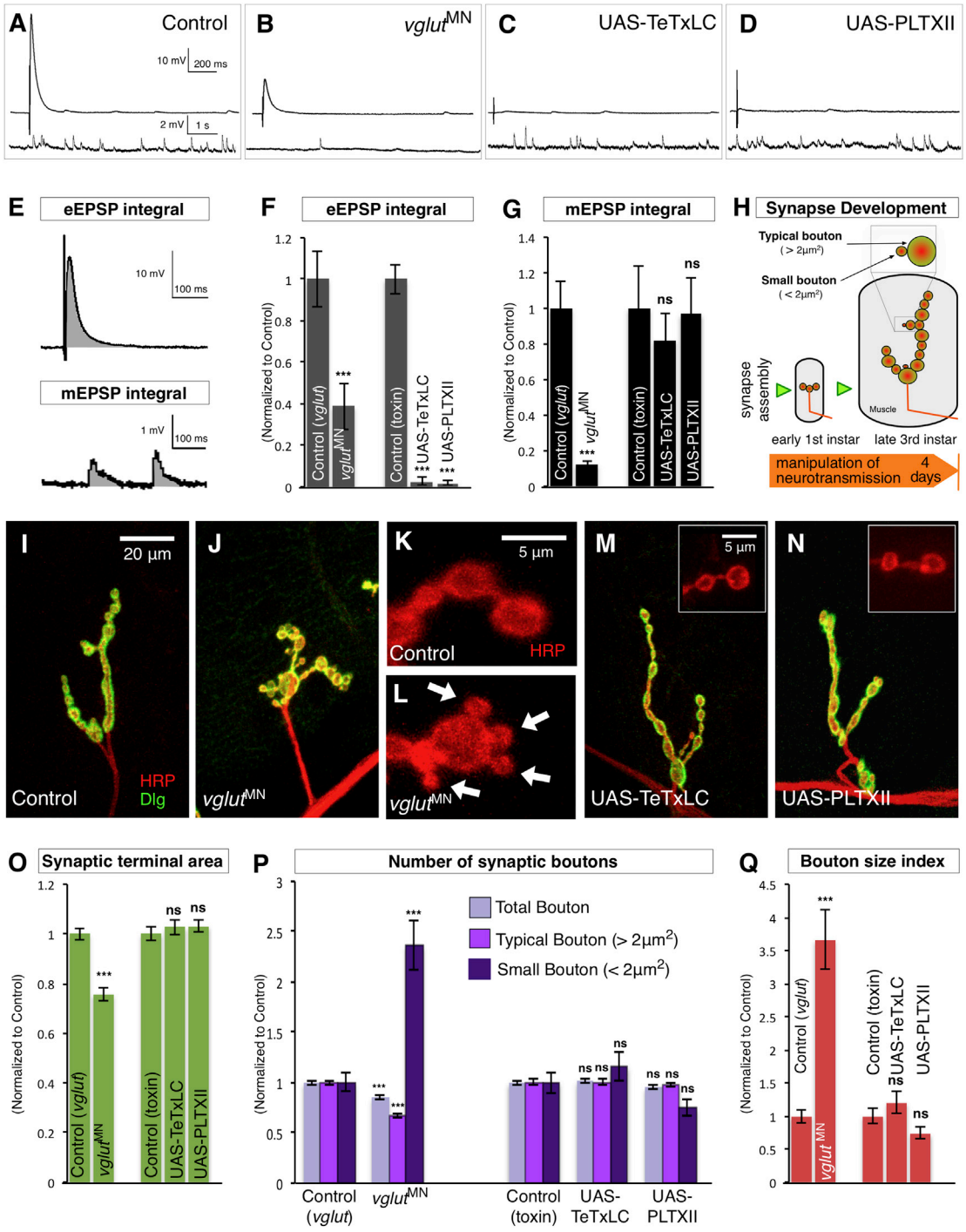

Figure 1. Neurotransmission Is Required for Larval Synaptic Terminal Development

(A–D) Representative traces of eEPSPs (above) and mEPSPs (below) from (A) control (CS), (B) *vglut*^{MN} (*vglut*$^{Hypo/Df}$,*UAS-Vglut-RNAi*^{KK};*D42-Gal4*/*UAS-Vglut-RNAi*^{JF}), (C) UAS-TeTxLC (*OK319-Gal4*/*UAS-TeTxLC*), and (D) UAS-PLTXII (*OK6-Gal4*/+;+/*UAS-PLTXII*).

(E) Representation of measurement of eEPSP integral (above) and mEPSPs integral (below).

(F and G) Quantification of (F) eEPSP integral (n ≥ 6) and (G) mEPSPs integral (n ≥ 9) of the indicated genotypes.

(H) Schematic of *Drosophila* larval neuromuscular junction synaptic terminal development during the experimental period.

(I–N) Representative NMJ terminals and individual boutons (K and L, insets of M and N) labeled with the postsynaptic marker Dlg (green) and the neuronal membrane marker horseradish peroxidase (HRP) (red). Arrows indicate small boutons (L).

(legend continued on next page)

release, we generated a transgenic membrane-tethered version of Plectreurys toxin II (UAS-PLTXII), which blocks the *Drosophila* synaptic N-type voltage-gated calcium channel Cacophony that is essential for evoked release (Wu et al., 2008). Similar to TeTxLC, expression of PLTXII in MNs dramatically reduced evoked release but did not significantly alter miniature NT (Figures 1D, 1F, 1G, and S2B–S2D). We assessed the effects of expression of both of these toxins on synaptic terminal development (Figures 1M and 1N). We found no change of synaptic terminal area, the number of synaptic boutons, or the bouton size index at these terminals compared to controls (Figures 1O–1Q). Therefore, using these criteria, evoked neurotransmission is not required for normal synaptic structural development.

Miniature Neurotransmission Is Required for Synaptic Terminal Development

Our results indicated that while the inhibition of both evoked and miniature neurotransmission in $vglut^{MN}$ mutants perturbed synaptic development, blocking evoked release alone was not detrimental. We therefore hypothesized that miniature NT could be particularly required for synapse development or alternatively that synapse development relied upon the total amount of NT regardless of whether it was derived from evoked or miniature events. To discriminate between these hypotheses, we sought genetic conditions where miniature NT could be preferentially reduced versus evoked NT. To do this, we took advantage of the phenomena of synaptic homeostasis that occurs at both *Drosophila* and mammalian synapses (Davis, 2013; Turrigiano, 2012). When postsynaptic ionotropic glutamate receptors (iGluRs) are reduced at *Drosophila* NMJ synapses, presynaptic terminals increase the number of synaptic vesicles released (quantal content) per action potential in order to maintain synaptic strength (Frank et al., 2006; Petersen et al., 1997). We exploited this process in mutant combinations where iGluR function was severely inhibited to specifically reduce miniature NT.

As a starting point, we employed iGluR mutants (Schmid et al., 2006) where the expression levels of endogenous glutamate receptor subunits were severely depleted (Figure S3A). In order to avoid disrupting the synaptic scaffolding functions of iGluRs, we combined these mutants with genomic promoter-driven rescuing transgenes. These transgenes produced either a wild-type glutamate receptor subunit ($iGluR^{WT}$ combination) or a subunit where the glutamate binding region was mutated (Schmid et al., 2006), rendering the receptor nonfunctional ($iGluR^{MUT}$ combination) (Figure S3A). Synaptic levels of both $iGluR^{WT}$ and $iGluR^{MUT}$ receptor clusters were similar when measured using an independent obligate iGluR subunit (dGluRIIC) (Figures S3B–S3D). We then measured NT in these mutants. $iGluR^{WT}$ terminals had similar miniature NT to controls (Figures 2A, 2B, 2F, S3F, and S3G). In contrast, $iGluR^{MUT}$ terminals had severely reduced miniature NT with a 96% ($p < 0.001$) reduction of the mEPSP integral (Figures 2C, 2F, S3F, and S3G) compared to controls. Miniature NT defects in $iGluR^{MUT}$ mutants were fully rescued by postsynaptic expression of a wild-type iGluR subunit (UAS-$dGluR^{WT}$) (Figures 2D and 2F). Though both $iGluR^{WT}$ and $iGluR^{MUT}$ had reduced evoked NT compared to background controls, importantly, they had similar evoked NT to each other (Figures 2A–2C, 2E, and S3E). As predicted, this was due to an increase in quantal content at $iGluR^{MUT}$ terminals compared to $iGluR^{WT}$ terminals (Figure S3H). To determine if this homeostatic compensation occurred throughout larval synaptic development, we also measured NT of $iGluR^{WT}$ and $iGluR^{MUT}$ first-instar larval terminals. Just as in later animals, we found that evoked NT was similar while miniature NT was reduced in $iGluR^{MUT}$ mutants compared to $iGluR^{WT}$ (Figures S3I–S3N). Therefore, during synaptic development, miniature NT is specifically reduced at $iGluR^{MUT}$ terminals compared to $iGluR^{WT}$ terminals, while evoked NT remains similar.

We next examined the synaptic terminal morphology of $iGluR^{MUT}$ and $iGluR^{WT}$ combinations. We found that $iGluR^{MUT}$ mutants had aberrant terminals with decreased synaptic terminal area and dramatic 443% increase ($p < 0.001$) of the bouton size index (Figures 2G, 2H, 2J, and 2K) compared to $iGluR^{WT}$ terminals. $iGluR^{WT}$ terminal morphology was similar to controls (Figures 2G–2J). The synaptic defects of $iGluR^{MUT}$ terminals were strikingly similar to those of $vglut^{MN}$ mutants (Figure 1L) and were rescued by postsynaptic expression of UAS-$dGluR^{WT}$ (Figures 2G, 2H, and 2L). In addition, though homeostatic compensation was active at $iGluR^{MUT}$ terminals, their aberrant morphology was unaltered by the postsynaptic activation or inhibition of the homeostasis regulator CamKII (Figures S4A and S4B) (Haghighi et al., 2003), indicating these morphological defects were not dependent upon synaptic homeostasis mechanisms. Therefore, the specific synaptic morphology defects of $iGluR^{MUT}$ mutants compared to $iGluR^{WT}$ supported the hypothesis that miniature events had a unique role in synapse development.

The Role of Miniature Neurotransmission in Synapse Development Is Independent of Evoked Neurotransmission

To further investigate the specific role of miniature neurotransmission in synapse development, we next asked if the phenotypes induced by the loss of miniature events were independent of the amount of evoked NT. To do this, we first blocked evoked release together with miniature NT by MN expression of PLTXII in $iGluR^{MUT}$ mutants. This did not further alter miniature NT but, as expected, strongly inhibited evoked release (Figures 3A–3C, 3G, 3H, and S4D–S4F). In spite of this, the synaptic morphology in these animals was unchanged compared to $iGluR^{MUT}$ mutants alone (Figures 3I–3M). Expression of PLTXII in the MNs of $iGluR^{WT}$ also induced no morphological phenotypes (data not shown). Therefore, depleting evoked release in addition to miniature NT did not further disrupt synaptic morphology.

(O–Q) Quantification of the morphological features of NMJ synaptic terminals including (O) synaptic terminal area, (P) synaptic bouton number, and (Q) the bouton size index ($n \geq 30$) of the indicated genotypes.

All quantification data are normalized to control (Control [*vglut*]; $vglut^{Df/+}$); (Control [toxin]; CS). Scale is identical in (I), (J), (M), and (N); in (K) and (L); and in the insets of (M) and (N). All error bars indicate ±SEM. *$p < 0.05$, ***$p < 0.001$. See also Figures S1 and S2.

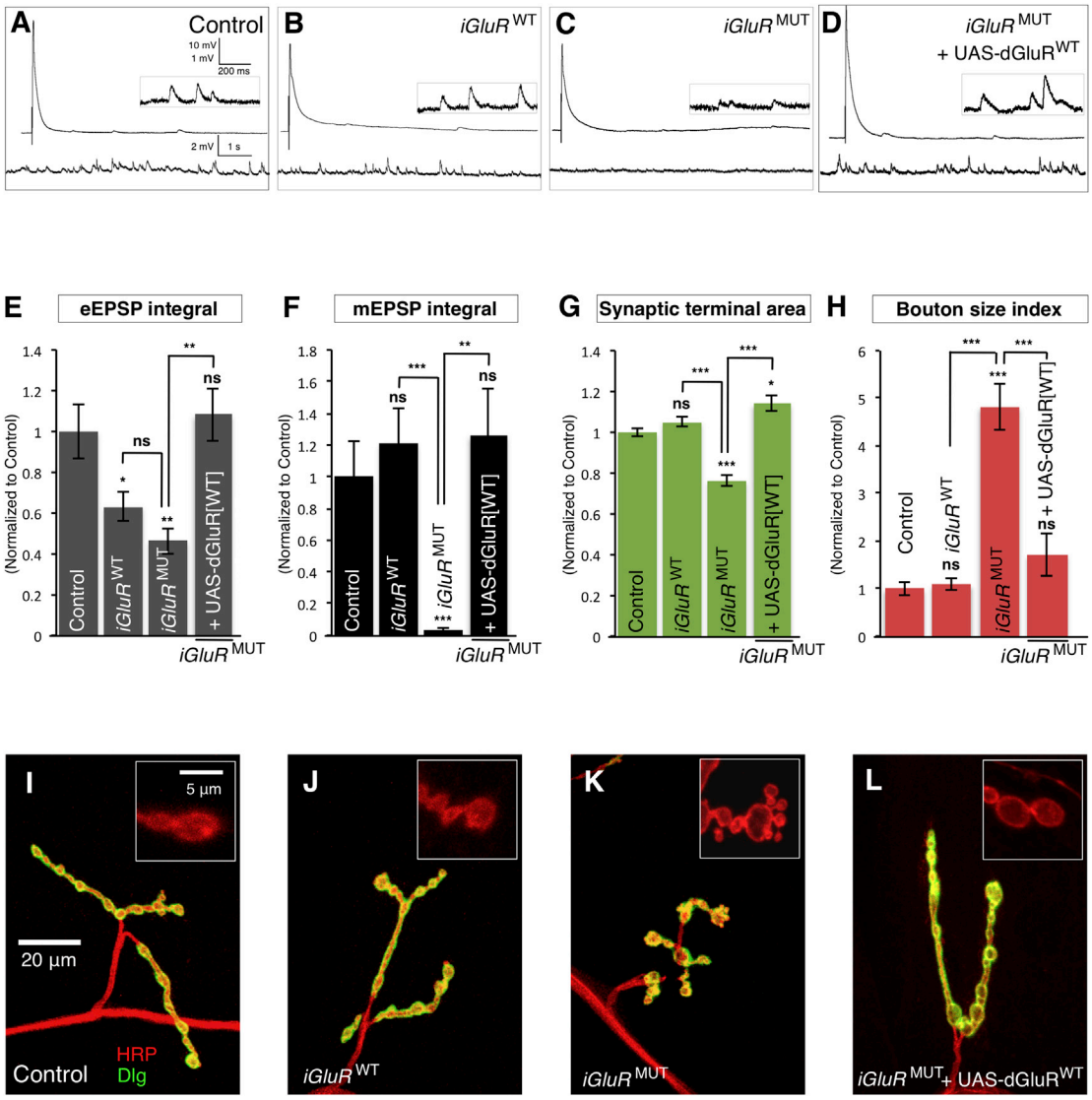

Figure 2. Miniature Neurotransmission Is Required for Normal Synaptic Terminal Development

(A–D) Representative traces of eEPSPs (above) and mEPSPs (below and inset) from (A) control (*dglurIIA*$^{+/-}$,*IIB*$^{Df/-}$), (B) *iGluR*^{WT} (*dglurIIA*$^{Hypo/-}$,*IIB*$^{Df/-}$;+/*genomic-dglurIIA*^{WT}), (C) *iGluR*^{MUT} (*dglurIIA*$^{Hypo/-}$,*IIB*$^{Df/-}$;+/*genomic-dglurIIA*^{E783A}), and (D) *iGluR*^{MUT}+UAS-dGluR^{WT} (*dglurIIA*$^{Hypo/-}$,*IIB*$^{Df/-}$,*G14-Gal4*;*UAS-dglurIIA*^{WT}/*genomic-dglurIIA*^{E783A}).

(E and F) Quantification of (E) eEPSP integral ($n \geq 8$) and (F) mEPSP integral ($n \geq 8$).

(G and H) Quantification of the NMJ (G) synaptic terminal area and (H) bouton size index ($n \geq 22$). All quantification data are normalized to control.

(I–L) Representative NMJ terminals and boutons (inset) labeled with Dlg (green) and HRP (red). Scale is the same in (I)–(L) and in the insets of (I)–(L).

Error bars indicate ±SEM. *$p < 0.05$, **$p < 0.01$, ***$p < 0.001$. See also Figures S3 and S4.

In a converse experiment, we asked if increasing evoked release could compensate for the decreased miniature NT in *iGluR*^{MUT} mutants. Evoked NT, unlike miniature NT, depends upon action potentials, which are induced by voltage-gated sodium channels. To specifically increase evoked NT without affecting miniature NT, we generated a transgenic membrane-tethered version of the Australian funnel-web spider peptide toxin delta-ACTX-Hv1a (UAS-δACTX), which prolongs the activation of the *Drosophila* voltage-gated sodium channel Para by inhibiting its inactivation (Wu et al., 2008). Expression of δACTX in the MNs of control animals increased the amount of evoked NT by prolonging the duration of eEPSPs (Figure S4C). When we expressed δACTX in the MNs of *iGluR*^{MUT} mutants, we also observed prolonged eEPSPs (Figure 3D) resulting in a 78% ($p < 0.05$) increase of evoked NT but no change of miniature NT (Figures 3G, 3H, and S4D–S4F). Nonetheless, when we examined the synaptic terminals of *iGluR*^{MUT} mutants expressing δACTX, we observed no change of synaptic terminal area or the bouton size index compared to *iGluR*^{MUT} mutants alone (Figures 3I, 3J, and 3N). This indicated that increasing evoked

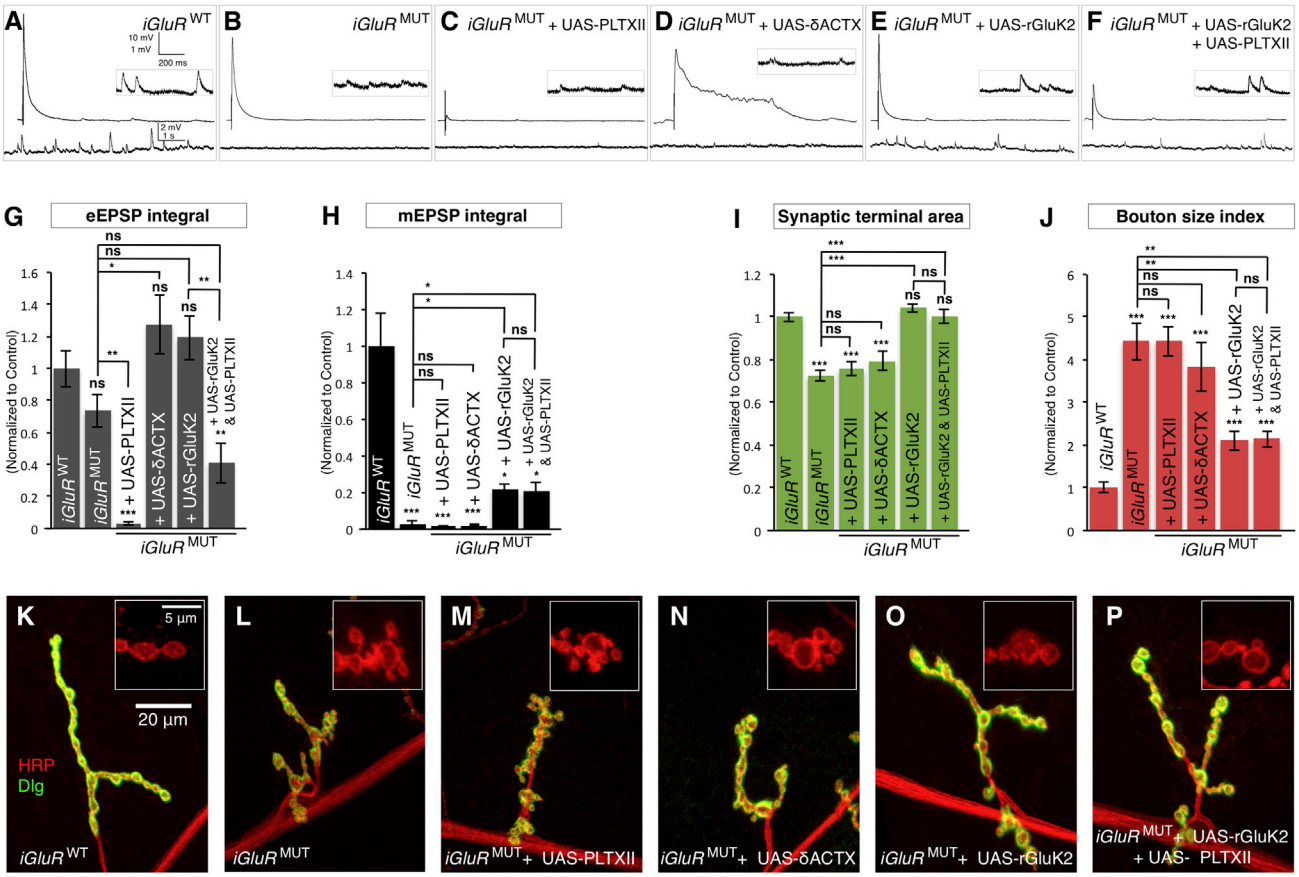

Figure 3. The Requirement of Miniature Neurotransmission for Synapse Development Is Independent of Evoked Neurotransmission and Requires Ionotropic Glutamate Receptor Activity

(A–F) Representative traces of eEPSPs (above) and mEPSPs (below and inset) from (A) *iGluR*^{WT} (*dglurIIA*$^{Hypo/-}$,*IIB*$^{Df/-}$;+/*genomic-dglurIIA*^{WT}), (B) *iGluR*^{MUT} (*dglurIIA*$^{Hypo/-}$,*IIB*$^{Df/-}$;+/*genomic-dglurIIA*^{E783A}), (C) *iGluR*^{MUT} + UAS-PLTXII (*dglurIIA*$^{Hypo/-}$,*IIB*$^{Df/-}$,*OK319-Gal4*;*UAS-PLTXII*/*genomic-dglurIIA*^{E783A}), (D) *iGluR*^{MUT} + UAS-δACTX (*dglurIIA*$^{Hypo/-}$,*IIB*$^{Df/-}$,*OK319-Gal4*;*UAS-δACTX*/*genomic-dglurIIA*^{E783A}), (E) *iGluR*^{MUT} + UAS-rGluK2 (*dglurIIA*$^{Hypo/-}$,*IIB*$^{Df/-}$,*G14-Gal4*;*UAS-rGluK2*/*genomic-dglurIIA*^{E783A},*UAS-PLTXII*), and (F) *iGluR*^{MUT} + UAS-rGluK2 + UAS-PLTXII (*dglurIIA*$^{Hypo/-}$,*IIB*$^{Df/-}$,*G14-Gal4*,*OK319-Gal4*;*UAS-rGluK2* /*genomic-dglurIIA*^{E783A},*UAS-PLTXII*).

(G and H) Quantification of (G) eEPSP integral ($n \geq 8$) and (H) mEPSP integral ($n \geq 8$).

(I and J) Quantification of the NMJ (I) synaptic terminal area and (J) bouton size index ($n \geq 27$). All quantification data are normalized to control (*iGluR*^{WT}).

(K–P) Representative NMJ terminals and boutons (inset) labeled with Dlg (green) and HRP (red). Scale is the same in (K)–(P) and in the insets of (K)–(P).

Error bars indicate ±SEM. *$p < 0.05$, **$p < 0.01$, ***$p < 0.001$. See also Figure S4.

NT could not rescue synaptic defects induced by the depletion of miniature events. Congruously, we also found no change of synapse morphology when evoked NT was specifically increased or decreased in *vglut* hypomorphic mutants (Figures S4I–S4L). We conclude, therefore, that the role of miniature neurotransmission in synapse development is distinct from and cannot be compensated by evoked release.

Ionotropic Glutamate Receptor Activity Induced by Miniature Events Is Essential for Synapse Development

Presynaptic depletion of vesicular glutamate transporters or postsynaptic disruption of glutamate binding to receptors perturbs synapse morphology. This suggested that the release or detection of glutamate from miniature events was critical for normal synaptic development. To determine if the subsequent ionotropic activity of receptors in response to glutamate was also required, we sought to restore mEPSPs independently of endogenous receptors. To do this, we generated a *Drosophila* transgene of the rat kainate-type ionotropic glutamate receptor subunit GluR6/GRIK2/GluK2 (UAS-rGluK2). This mammalian receptor can form functional homotetrameric channels in heterologous systems (Egebjerg et al., 1991; Kauwe and Isacoff, 2013). We found that rGluK2 localizes to the *Drosophila* postsynapse when expressed in muscle, though it was not concentrated at active zones unlike endogenous receptors (Figures S4M and S4N). Postsynaptic expression of rGluK2 in control animals did not disrupt synapse morphology (data not shown). When we expressed rGluK2 in the postsynapse of *iGluR*^{MUT} mutants, we found this increased the mEPSP integral >7-fold ($p < 0.05$) compared to *iGluR*^{MUT} mutants alone (Figures 3E and 3H). The eEPSP integral was also increased, though this did not reach significance (Figures 3E and 3G). When we

examined the synaptic terminals of these animals, we found that the synaptic terminal area was fully restored to control size and the aberrant bouton size index was reduced by 53% ($p < 0.01$) (Figures 3I, 3J, and 3O). This result indicated that ionotropic activity of glutamate receptors was essential for synapse development.

To establish if the rescue ability of rGluK2 specifically depended upon miniature NT, we coexpressed PLTXII in MNs in *iGluR*^{MUT} mutants together with postsynaptic rGlurK2. This combination did not alter miniature NT but strongly reduced evoked release ($p < 0.01$) (Figures 3F–3H) compared to *iGluR*^{MUT} mutants expressing rGluK2 alone. However, the inhibition of evoked NT did not inhibit any aspect of the morphological rescue of *iGluR*^{MUT} mutants by rGluK2 (Figures 3I, 3J, 3O, and 3P). Expression of PLTXII or rGluK2 in either the pre- or postsynapse of controls did not alter terminal morphology (Figures S4G and S4H; data not shown). This finding further supported a singular requirement for miniature NT in terminal development. We conclude that the ionotropic activity of postsynaptic glutamate receptors, triggered by miniature events, is required for synapse growth.

Increasing Miniature Neurotransmission Promotes Synaptic Terminal Expansion

Because our results established that reduction of miniature neurotransmission inhibited synaptic development, we next investigated if increasing these events could also change synapse morphology. Complexin proteins bind to neuronal SNARE complexes and regulate neurotransmitter release (Brose, 2008). Mutants of *Drosophila* complexin (*cpx*) have a dramatic increase in spontaneous synaptic vesicle release and have increased numbers of synaptic boutons (Huntwork and Littleton, 2007). We hypothesized that these two phenotypes could be causally related through increased miniature NT. To test this idea, we first measured evoked and miniature NT in *cpx* null mutants. We found no change in the eEPSP integral (Figures 4A, 4B, and 4H) in these mutants, although eEPSP amplitudes were reduced compared to controls (Figure S5A), consistent with previous studies (Huntwork and Littleton, 2007; Iyer et al., 2013). In contrast, *cpx* mutants had a dramatic 81-fold increase ($p < 0.001$) in miniature NT (Figures 4A, 4B, and 4I). Expression of a complexin transgene (UAS-Cpx) in MNs rescued *cpx* mutants, restoring miniature NT to control levels (Figures 4C and 4I). When we measured the terminal morphology of *cpx* mutants, we observed a 44% increase ($p < 0.001$) in terminal area (Figures 4J, 4L, and 4M) accompanied by a 32% increase ($p < 0.001$) in typical bouton numbers but a 47% ($p < 0.01$) decrease in the number of small boutons (Figures S5B and S5C). This lead to a 64% decrease ($p < 0.001$) of the bouton size index (Figure 4K). As with neurotransmission, rescue of *cpx* mutants with transgenic complexin restored terminal area and the bouton size index (Figures 4J, 4K, and 4N). Therefore, *cpx* mutants have larger synaptic terminals with a decreased fraction of small boutons, the inverse of *vglut*^{MN} and *iGluR*^{MUT} mutant phenotypes.

We next wished to determine if evoked NT contributed to *cpx* mutant terminal phenotypes. We first analyzed the *cpx*^{1257} mutant allele, which has normal eEPSP amplitudes and kinetics (Iyer et al., 2013) (Figure S5A) but has similarly increased miniature NT to *cpx* null alleles (Figures 4B, 4D, and 4I). We found that *cpx*^{1257} mutants had increased terminal areas with a decreased bouton size index not significantly different from *cpx* null alleles (Figures 4J, 4K, and 4O). This indicated that the aberrant terminal overgrowth of *cpx* mutants was not due to abnormal evoked release. As a second test, we expressed PLTXII in MNs of *cpx* null mutants. As expected, this strongly inhibited evoked NT without significantly altering miniature events (Figures 4E, 4H, and 4I). When we measured the terminal morphology of these animals, we found no change compared to *cpx* mutants alone (Figures 4J, 4K, and 4P). Therefore, evoked NT is not required for the synaptic overgrowth of *cpx* mutants.

We next asked if increased miniature events are necessary for *cpx* mutant terminal overgrowth. We reduced miniature NT by expressing either a dominant-negative glutamate receptor subunit (UAS-dGluR^{DN}) (Schmid et al., 2006) in postsynaptic muscles or an RNAi against *vglut* (RNAi-Vglut) in the presynaptic MNs of *cpx* mutants (Figures 4F and 4G) and controls (Figures S5D and S5E). Both manipulations did not significantly alter evoked NT in *cpx* mutants but did decrease miniature NT (Figures 4F–4I). In both conditions, we found that the aberrant synaptic terminal area and bouton size indexes of *cpx* mutants were suppressed (Figures 4J, 4K, 4Q, and 4R). Thus, the inhibition of miniature NT suppressed the terminal overgrowth of *cpx* mutants while the depletion of evoked NT did not. Therefore, increased miniature neurotransmission, as found in *complexin* mutants, is sufficient to promote synaptic terminal growth.

Individual Bouton Expansion Is Bidirectionally Regulated by Miniature Neurotransmission

cpx mutants had opposing synaptic morphological changes to *vglut*^{MN} and *iGluR*^{MUT} mutants. This was most apparent in the bidirectional effect upon bouton size, with *vglut*^{MN} and *iGluR*^{MUT} mutants having an increase in the proportion of small boutons and *cpx* mutants oppositely having a decreased fraction of these boutons. During terminal development, new synaptic boutons are added and then expand and may also be eliminated (Koch et al., 2008; Zito et al., 1999). A defect in one or more of these steps could potentially result in the changes to bouton sizes we observed when miniature NT was altered. We sought therefore to visualize the development of individual synaptic boutons by time-lapse live imaging through the transparent cuticle of intact larvae. To do this, we utilized the LexA binary system to express a membrane-localized GFP in the presynaptic terminals of both control and miniature NT mutants. Beginning 24 hr after hatching, we anesthetized animals every 24 hr for 4 days during larval development and imaged their synaptic terminals, returning them to food media between imaging periods.

Using this technique, we found that new synaptic boutons formed continuously throughout the imaging period in control and NT mutant backgrounds at the same rate (Figures S6A and S6B). In control animals, 94.4% (34/36) of newly formed small boutons (<2 μm^2) then became progressively larger over time to become typical-sized boutons (>2 μm^2) during the imaging period (Figures 5A and 5G). This expansion in size was not perturbed by inhibiting evoked NT using TeTxLC (Figures 5B and 5G). However, in *iGluR*^{MUT} mutants, where miniature NT

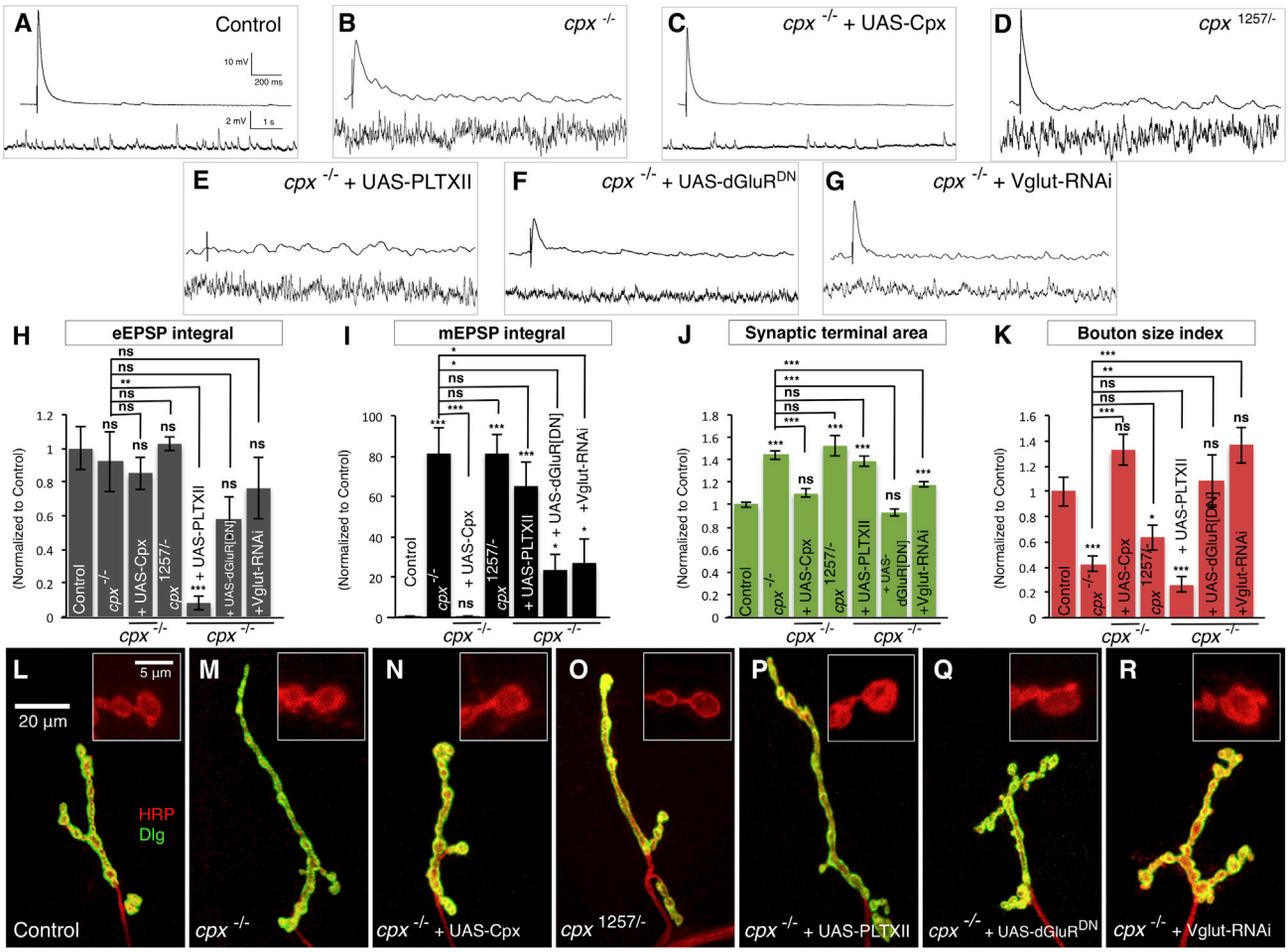

Figure 4. Increasing Miniature Neurotransmission Promotes Synaptic Terminal Expansion

(A–G) Representative traces of eEPSPs (above) and mEPSPs (below) from (A) control ($cpx^{Df/+}$), (B) $cpx^{-/-}$ mutant ($cpx^{Df/-}$), (C) $cpx^{-/-}$ + UAS-Cpx (*UAS-Cpx/+;OK6-Gal4/+;cpx*$^{Df/-}$), (D) $cpx^{1257/-}$ mutant ($cpx^{Df/1257}$), (E) $cpx^{-/-}$ + UAS-PLTXII (*UAS-PLTXII/OK319-Gal4;cpx*$^{Df/-}$), (F) $cpx^{-/-}$ + UAS-dGluR^{DN} (*G14-Gal4/+;cpx*$^{Df/-}$*,UAS-dglurIIA*^{E783A}), and (G) $cpx^{-/-}$ + Vglut-RNAi (*UAS-Vglut-RNAi*^{KK}*/OK6-Gal4;cpx*$^{Df/-}$).

(H and I) Quantification of (H) eEPSP integral ($n \geq 8$) and (I) mEPSP integral ($n \geq 11$).

(J and K) Quantification of the NMJ (J) synaptic terminal area and (K) bouton size index ($n \geq 23$). All quantification data are normalized to control.

(L–R) Representative NMJ terminals and boutons (inset) labeled with Dlg (green) and HRP (red). Scale is the same in (L)–(R) and in the insets of (L)–(R).

Error bars indicate ±SEM. *$p < 0.05$, **$p < 0.01$, ***$p < 0.001$. See also Figure S5.

was reduced, we found that the enlargement of small boutons was severely retarded compared to *iGluR*^{WT} animals (Figures 5C, 5D, and 5H) and only 19.6% (10/51) of small boutons ever expanded to become typical-sized boutons. In contrast, in *cpx* mutants where miniature NT was increased, the rate of expansion of small boutons to typical boutons was accelerated compared to controls (Figures 5E, 5F, and 5I). The effect on individual bouton growth of increasing or decreasing miniature NT was similar regardless of whether new boutons formed at early, intermediate, or late stages during the 4-day imaging period (Figures S6C–S6H). Finally, we saw no change in the low frequency of elimination of existing boutons in any NT mutant compared to controls (Figures S6I and S6J). Thus, the enlargement of individual synaptic boutons was stalled when miniature NT was inhibited and conversely was accelerated when miniature NT was increased. This modification of the growth properties of individual boutons by altering miniature NT was consistent with the changes we observed of bouton size indexes. These results established that the growth process of individual synaptic boutons was discretely regulated by miniature neurotransmission.

Synapse Maturation Is Regulated by Miniature Neurotransmission

In control animals, ~95% of all small boutons expand to become larger, and our data demonstrated a failure of this process in the majority of boutons when miniature neurotransmission was depleted. We speculated that this morphological change of boutons could be associated with other important features of synaptic maturation. To investigate this, we first compared the synaptic ultrastructure of small (<2 μm^2) and typical boutons (>2 μm^2) in wild-type animals. We found that both bouton categories were grossly similar with clearly discernable synaptic

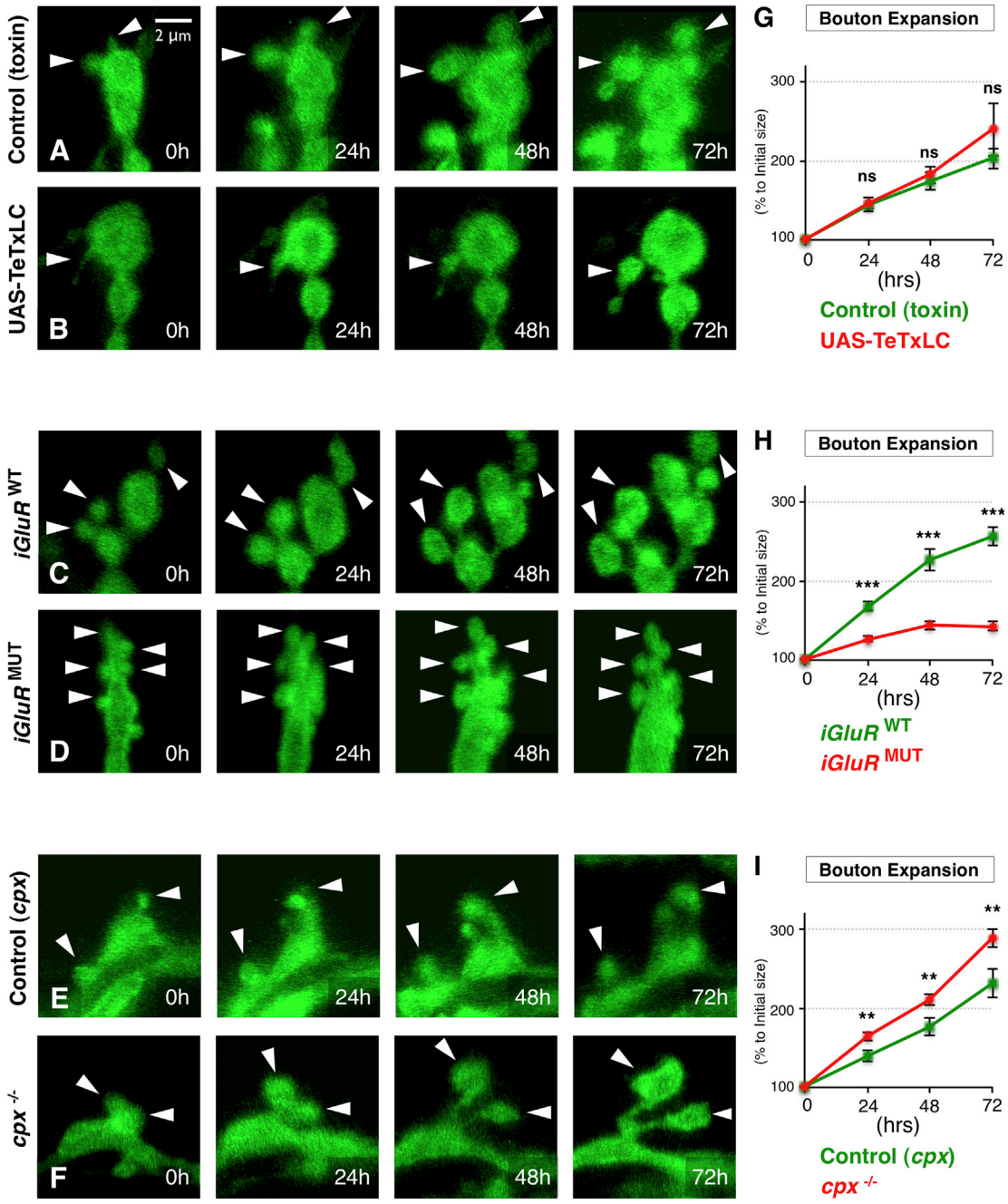

Figure 5. Individual Bouton Expansion Is Bidirectionally Regulated by Miniature Neurotransmission

(A–F) Representative time-lapse images from live animals of synaptic boutons labeled with membrane tagged GFP at muscles 1 or 9 captured every 24 hr during larval development beginning 24 hr after hatching. Small boutons formed before 0 hr and tracked over the imaging period are indicated by arrowheads. Genotypes (A) control(toxin) (*Vglut-lexA,LexOp-CD8-GFP/+*), (B) UAS-TeTxLC (*OK319-Gal4/UAS-TeTxLC;Vglut-lexA,LexOp-CD8-GFP/+*), (C) *iGluR*^{WT} (*dglurIIA*$^{Hypo/-}$,*IIB*$^{Df/-}$;*Vglut-lexA,LexOp-CD8-GFP/genomic-dglurIIA*^{WT}), (D) *iGluR*^{MUT} (*dglurIIA*$^{Hypo/-}$,*IIB*$^{Df/-}$;*Vglut-lexA,LexOp-CD8-GFP/genomic-dglurIIA*^{E783A}), (E) control (*cpx*) (*Vglut-lexA,LexOp-CD8-GFP,cpx*$^{Df/+}$), and (F) *cpx*$^{-/-}$ mutant (*cpx*$^{Df/-}$,*Vglut-lexA,LexOp-CD8-GFP*). Scale is the same for all images.

(G–I) Quantification of the bouton size expansion during the time-lapse imaging period (n ≥ 35 boutons for G, n ≥ 51 boutons for H, and n ≥ 42 boutons for I, from n ≥ 7 NMJs).

All data are normalized to initial bouton size. Error bars indicate ±SEM. *p < 0.05, **p < 0.01, ***p < 0.001. See also Figure S6.

hallmarks including mitochondria, presynaptic vesicle clusters, synaptic clefts, and postsynaptic elaborations (Figures 6A and 6C). However, we found that T-bars, the electron-dense presynaptic specializations required for efficacy of evoked release at *Drosophila* synapses (Kittel et al., 2006), were different between the active zones of typical and small boutons. While in typical

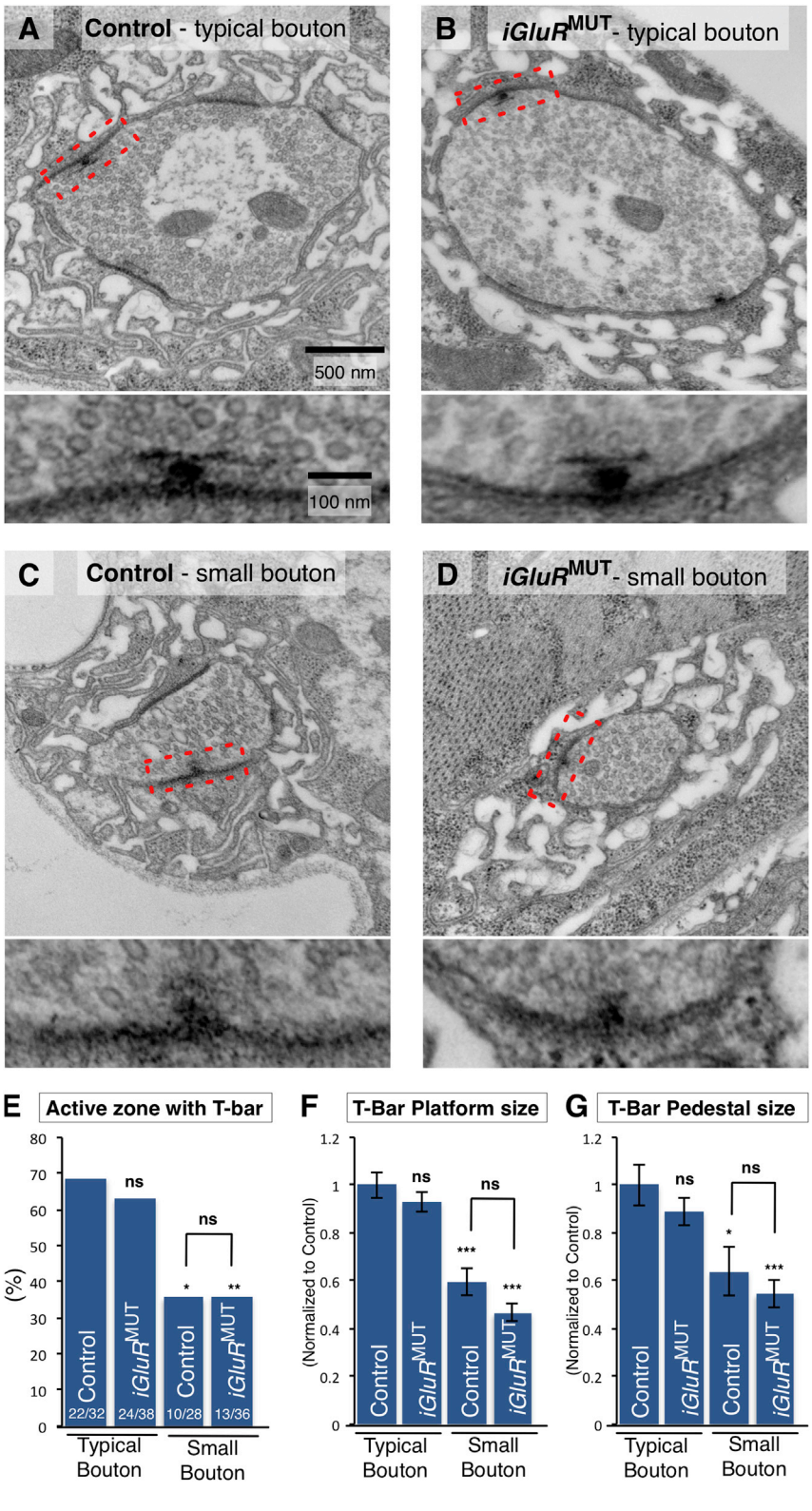

Figure 6. Synaptic Active-Zone Maturation Is Regulated by Miniature Neurotransmission

(A and B) Representative micrographs of synaptic boutons (above) and active zones (box above, inset below) from a typical-size bouton of (A) control (CS) and (B) *iGluR*^{MUT} mutants.

(C and D) Representative micrographs of small boutons from (C) control and (D) *iGluR*^{MUT}.

(E–G) Quantification of (E) the active-zone occurrence, (F) T-bar platform size, and (G) T-bar pedestal size ($n \geq 10$). Quantification data are normalized to control (F and G).

Scale is the same in (A)–(D) and in the insets of (A)–(D). Error bars indicate ±SEM. *$p < 0.05$, * $p < 0.01$, ***$p < 0.001$.

boutons 69% of active zones had a T-bar present, only 36% of active zones in small boutons had an electron-dense presynaptic structure (Figure 6E). Furthermore, the structures present at small bouton active zones were primitive, irregularly shaped (Figures 6A and 6C, insets), and smaller than those at the active zones of typical boutons (Figures 6F and 6G). These results indicated that synaptic ultrastructure is less developed in small boutons compared to typical boutons in wild-type animals.

We then examined the synaptic ultrastructure in *iGluR*^{MUT} mutant terminals and compared them to controls. We found no ultrastructure differences between the typical boutons of *iGluR*^{MUT} mutants and the typical boutons of controls, including the features of active zones and T-bars (Figures 6A, 6B, and 6E–6G). However, we found that the numerous small boutons in *iGluR*^{MUT} mutants had immature active-zone features similar to those of small boutons in wild-type animals, including reduced T-bar frequency, rudimentary T-bar structure, and reduced T-bar size (Figures 6C–6G). These data, combined with live-imaging results, suggest that inhibition of miniature NT interrupts synaptic development resulting in boutons becoming stalled in an immature state, reminiscent of the normally transient small boutons of wild-type animals. These results are consistent with miniature neurotransmission also being necessary for synaptic ultrastructural maturation in addition to morphological expansion.

Miniature Neurotransmission Acts Locally to Regulate Synapse Development

We next sought to establish the nature of the developmental signal induced by miniature neurotransmission. Synaptic structure can be influenced by factors that act locally at the individual terminal level (e.g., synaptic adhesion factors; Davis and Goodman, 1998) or

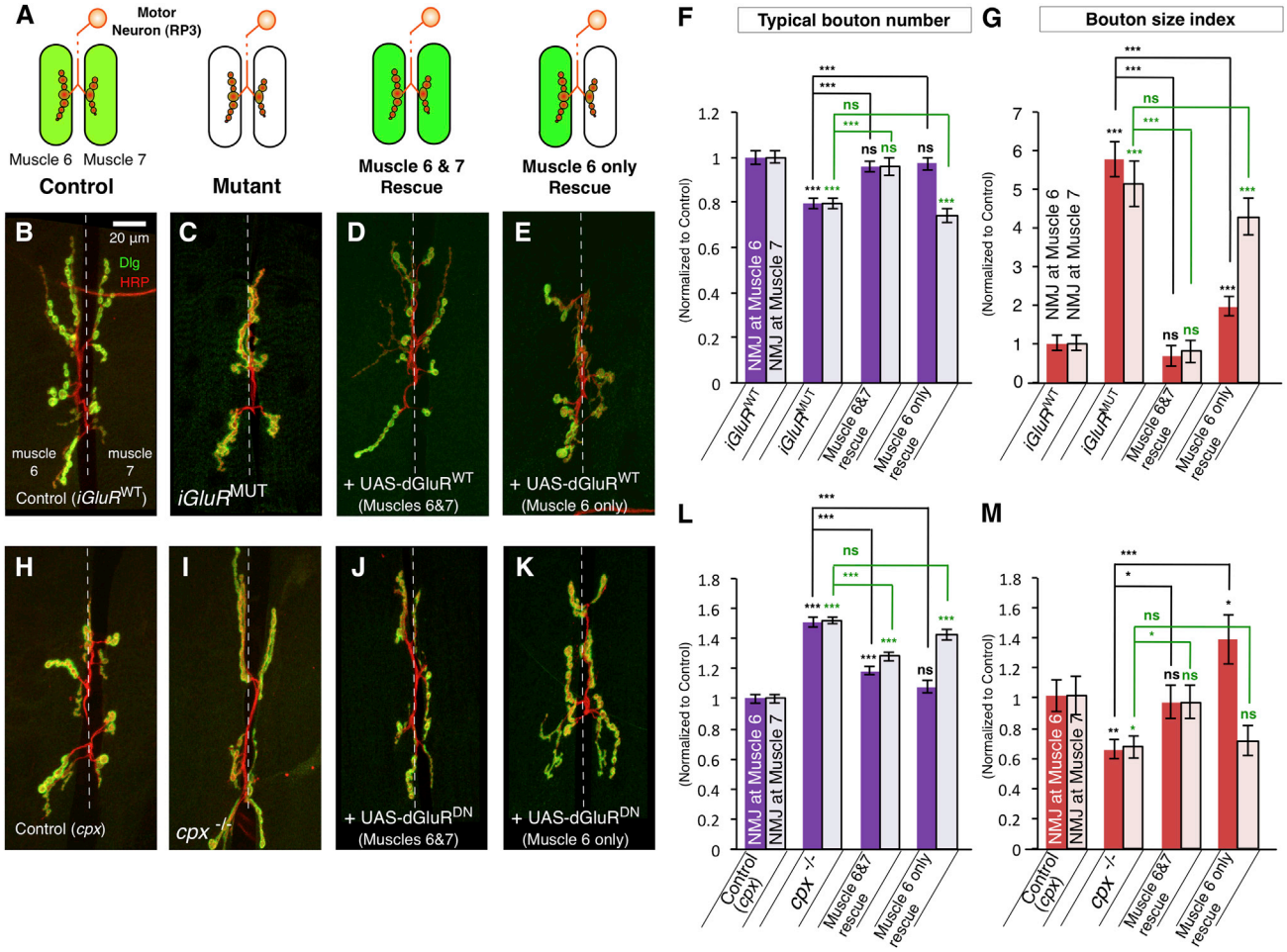

Figure 7. Miniature Neurotransmission Acts Locally to Regulate Bouton Development

(A) Schematic of the two separate synaptic terminals on muscles 6 and 7 generated by the single motor neuron RP3. Muscle Gal4 lines allow rescue of mutants at either both terminals at muscles 6 and 7 or the terminal at muscle 6 only.

(B–E and H–K) Representative NMJ terminals at muscles 6 and 7, segment A3, labeled with Dlg (green) and HRP (red) from (B) *iGluR*^{WT}, (C) *iGluR*^{MUT}, (D) *iGluR*^{MUT} + UAS-dGluR^{WT} (muscles 6 and 7) (*dglurIIA*$^{Hypo/-}$,*IIB*$^{Df/-}$;*C57-Gal4/genomic-dglurIIA*^{E783A},*UAS-dglurIIA*^{WT}), (E) *iGluR*^{MUT} + UAS-dGluR^{WT} (muscle 6 only) (*dglurIIA*$^{Hypo/-}$,*IIB*$^{Df/-}$;*H94-Gal4,nSyb-Gal80/genomic-dglurIIA*^{E783A},*UAS-dglurIIA*^{WT}), (H) control(*cpx*) (*cpx*$^{Df/+}$), (I) *cpx*$^{-/-}$ mutant, (J) *cpx*$^{-/-}$ + UAS-dGluR^{DN} (muscles 6 and 7) (*G14-Gal4/+;cpx*$^{Df/-}$,*UAS-dglurIIA*^{E783A}), and (K) *cpx*$^{-/-}$ + UAS-dGluR^{DN} (muscle 6 only) (*cpx*$^{Df/-}$,*UAS-dglurIIA*^{E783A},*H94-Gal4,nSyb-Gal80*).

(F, G, L, and M) Quantification of the typical bouton number (F and L) and bouton size index (G and M) from terminals at muscles 6 and 7 ($n \geq 32$). Statistical comparisons are labeled in black for terminal 6 and green for terminal 7.

All quantification data are normalized to control. Scale is the same for all images. Error bars indicate ±SEM. *$p < 0.05$, ***$p < 0.001$. See also Figure S7.

throughout the whole neuron (e.g., transcriptional regulation; McCabe et al., 2003). Action potentials and evoked NT affect the entire synaptic terminal. In contrast, we surmised that the effects of miniature NT might be spatially restricted to individual active zones and therefore could act locally to regulate bouton maturation. To test this hypothesis, we examined the synaptic terminals generated by the type Ib motor neuron RP3 (Hoang and Chiba, 2001). The single axon of this neuron bifurcates to produce synaptic terminals concurrently on two postsynaptic targets: muscle 6 and muscle 7 (Figure 7A). The ratio of synaptic boutons produced at each muscle is stereotyped (Davis and Goodman, 1998), and these muscles are not electrically coupled with each other (Ueda and Kidokoro, 1996), facilitating independent manipulation of NT. We used Gal4 drivers expressed either in muscle 6 alone (but not muscle 7) (Figures 7A and S7A) or in both muscles to dissect if miniature NT signaling acts locally at terminals or throughout the neuron.

Similar to other synapses, reduction of miniature NT by *iGluR*^{MUT} reduced typical bouton numbers (Figures 7B, 7C, and 7F) and increased the fraction of small boutons (Figure 7G) at both of the RP3 MN terminals on muscles 6 and 7 compared to controls, though the area of these terminals could not be accurately measured due their complex spatial arrangement. When we overexpressed a wild-type iGluR transgene (UAS-dGluR^{WT}) in both postsynaptic muscles of *iGluR*^{MUT} mutants, we restored normal miniature NT at both terminals (Figure S7B). This also fully rescued bouton numbers and the bouton size

index at both terminals (Figures 7D, 7F, and 7G). We next expressed UAS-dGluR^{WT} only in muscle 6 of *iGluR*^{MUT} mutants. This increased miniature NT at muscle 6 terminals without altering NT at muscle 7 (Figure S7B). When we examined the morphology of both terminals, we found that bouton numbers and bouton size were restored at terminals at muscle 6 (Figures 7E–7G). In contrast, however, the terminals at muscle 7 were not rescued (Figures 7E–7G). Because both terminals are produced by a single neuron, this result suggested that the effect of reduced miniature NT on synaptic bouton maturation is localized to individual terminals.

In a complementary experiment, we examined the suppression of *cpx* mutants using a similar strategy. *cpx* mutant terminals on both muscles 6 and 7 are expanded and the bouton size index was reduced compared to controls (Figures 7H, 7I, 7L, and 7M). When we expressed dominant-negative UAS-dGluR^{DN} in both postsynaptic muscles of these mutants, the excessive miniature NT at both terminals was strongly inhibited (Figure S7C). In both terminals, the aberrant number and size ratio of synaptic boutons were also suppressed (Figures 7J, 7L, and 7M). In contrast, when UAS-dGluR^{DN} was expressed only in muscle 6 of *cpx* mutants, miniature NT, bouton number, and bouton size index were only suppressed at the terminal on this muscle and not at the terminal on muscle 7 (Figures 7K–7M and S7C). Together, these experiments demonstrated that the effect on synapse maturation of increasing or decreasing miniature neurotransmission is via a mechanism that acts locally at synaptic terminals.

Miniature Neurotransmission Regulates Synapse Maturation through the GEF Trio and the GTPase Rac1

To determine the molecular mechanism through which miniature neurotransmission regulates bouton maturation, we next carried out a candidate mutant screen of molecules that were (1) linked to synapse morphological development and (2) likely to have localized activity at terminals. Among these candidates was Trio, a member of the evolutionarily conserved Dbl homology family of GEFs (Miller et al., 2013). *trio* mutants had previously been reported to have defective synaptic terminal growth (Ball et al., 2010), and Trio has been linked to the local regulation of the neuronal cytoskeleton (Miller et al., 2013). We confirmed that *trio* mutants had reduced numbers of synaptic boutons (Ball et al., 2010) (Figure S8A). We additionally found that *trio* mutants had reduced terminal area accompanied by large increase in the proportion of small boutons (Figures 8A, 8B, 8D, and 8E) very reminiscent of synaptic terminals when miniature NT is reduced (Figure 8C). All of these *trio* mutant synaptic phenotypes were fully rescued by presynaptic expression of transgenic Trio (UAS-Trio) (Figures 8D and 8E). When we examined the ultrastructure of the abundant small boutons in *trio* mutants, we found rudimentary T-bar structures (Figure 8G) of reduced size similar to those observed in the small boutons of miniature NT mutants (Figures 8H, S8C, and S8D). However, when we measured miniature NT in these mutants, we found it was unchanged compared to controls (Figure S8E), consistent with previous reports (Ball et al., 2010). This indicated that the synaptic terminal phenotypes in *trio* mutants did not originate from defective NT. However, the similarity of *trio* mutant synaptic morphology phenotypes to miniature NT mutant phenotypes suggested that Trio could be part of a molecular pathway triggered by miniature events.

Pursuing this hypothesis, we next tested the genetic interaction of miniature NT mutants with *trio* mutants. We first examined if Trio is required for the terminal overgrowth and bouton size alteration of *cpx* mutants. Double null mutants of *cpx* and *trio* had similarly increased miniature NT to *cpx* mutants alone (Figure S8F). However, when we examined the morphology of these double-mutant terminals, we found that synaptic terminal area and bouton size ratio were not different from *trio* mutants alone (Figures 8L–8N). Therefore, *cpx* mutant synaptic overgrowth was completely suppressed by the removal of *trio.* Furthermore, when we examined the terminal area and bouton size index of double mutants of *iGluR*^{MUT} and *trio*, they were also not different from *trio* mutant terminals alone (Figures S8G and S8H). Therefore, *iGluR*^{MUT} phenotypes are not genetically additive with *trio* mutant synaptic phenotypes. These results were consistent with Trio and miniature NT acting in a common molecular pathway regulating bouton development.

Building upon this result, we next examined if overexpression of Trio could rescue the effects of loss of miniature NT. When we overexpressed Trio in the MNs of *iGluR*^{MUT} mutants, we found no alteration of miniature NT compared to these mutants alone (Figure S8E). Nonetheless, when we examined the terminals of these animals, we found the synaptic terminal area was fully rescued to control levels and that the aberrant increased ratio of small boutons was suppressed by 44% ($p < 0.001$) (Figures 8O–8Q, 8T, and 8U). Overexpression of Trio in the presynapse of control animals caused a small increase in terminal area but no alteration of the bouton size ratio (Figures S8G and S8H). These results indicated that Trio acted as an essential "downstream" mediator of miniature NT in the regulation of bouton development.

Trio has previously been shown to activate the small GTPase Rac1 to modify the neuronal cytoskeleton (Ball et al., 2010; Miller et al., 2013). We therefore investigated if Rac1 also mediated the effects of miniature NT on synaptic development. Overexpression of either a transgenic wild-type Rac1 (UAS-Rac1^{WT}) or a GEF-independent activated mutant of Rac1 (UAS-Rac1^{ACT}) in the presynapse of controls induced a small change of terminal area and increased the bouton size index (Figures S8G and S8H). We then tested if these constructs could rescue the effects of reduced miniature NT. Presynaptic overexpression of UAS-Rac1^{WT} in *iGluR*^{MUT} mutants did not alter either synaptic terminal area or the bouton size index compared to *iGluR*^{MUT} mutants alone (Figures 8R, 8T, and 8U). However, presynaptic overexpression of UAS-Rac1^{ACT} in *iGluR*^{MUT} mutants fully rescued synaptic terminal area to control levels and reduced the aberrant bouton size index by 55% ($p < 0.001$) (Figures 8S–8U). This was comparable to rescue by presynaptic overexpression of Trio (Figures 8T and 8U). These results are consistent with Rac1 being activated by Trio in response to miniature NT in order to modulate synaptic development. Our results support a mechanism where miniature neurotransmission acts locally at synaptic terminals through a Trio-Rac1 signaling pathway to modify the synaptic cytoskeleton and promote structural maturation.

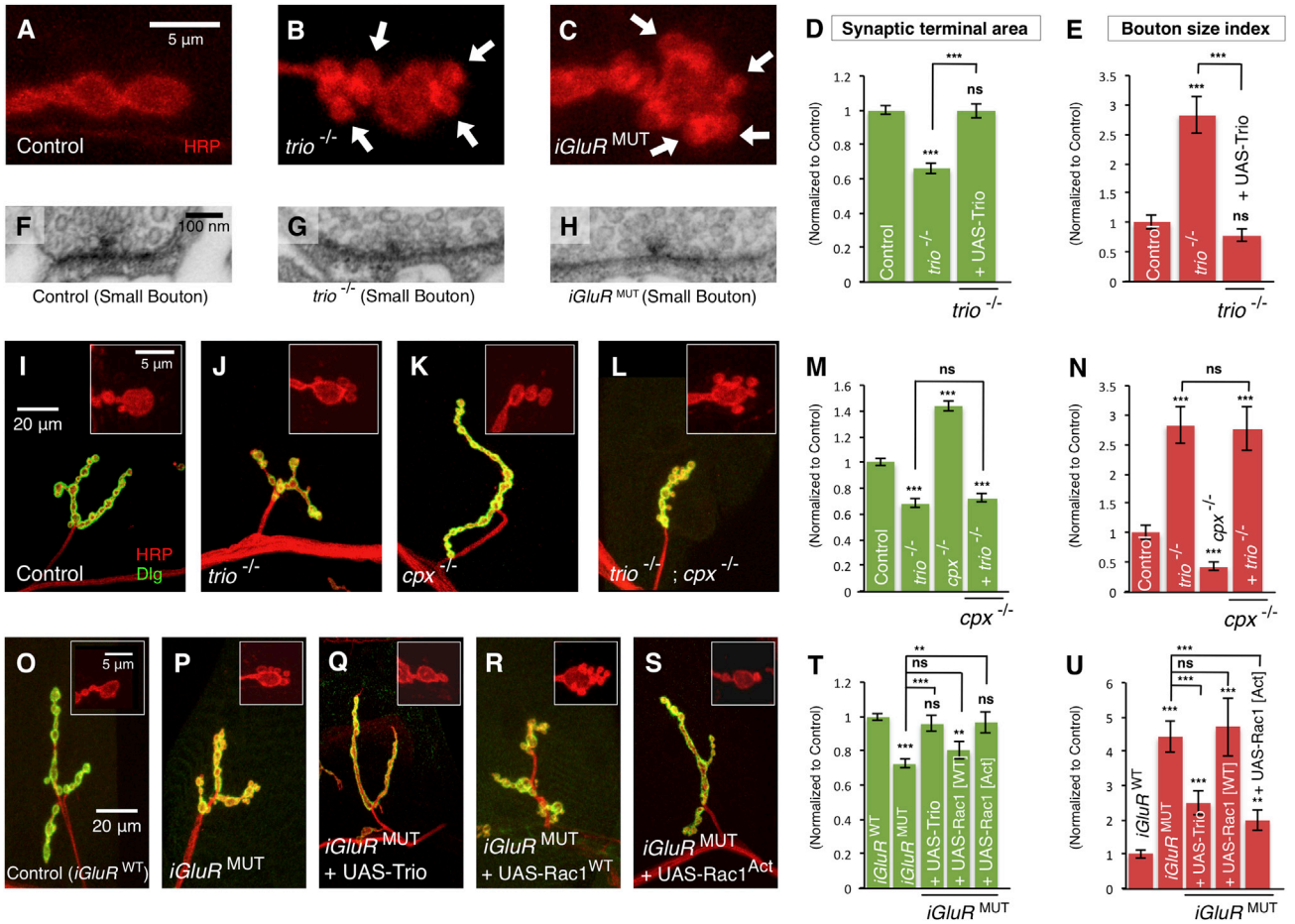

Figure 8. Miniature Neurotransmission Regulates Bouton Maturation through the GEF Trio and the Small GTPase Rac1

(A–C) Representative boutons of (A) control (CS), (B) *trio*$^{-/-}$ mutant, and (C) *iGluR*^{MUT} mutants.

(F–H) Representative micrographs of the active zone of small boutons of the indicated genotypes.

(I–L and O–S) Representative NMJ terminals and boutons (inset) from (I) control (CS), (J) *trio*$^{-/-}$ mutant, (K) *cpx*$^{-/-}$ mutant, (L) *trio*$^{-/-}$; *cpx*$^{-/-}$ mutants, (O) *iGluR*^{WT}, (P) *iGluR*^{MUT}, (Q) *iGluR*^{MUT} + UAS-Trio (*dglurIIA*$^{Hypo/-}$,*IIB*$^{Df/-}$,*OK319-Gal4*;*UAS-Trio/genomic-dglurIIA*^{E783A}), (R) *iGluR*^{MUT} + UAS-Rac1^{WT} (*dglurIIA*$^{Hypo/-}$, *IIB*$^{Df/-}$,*OK319-Gal4*;*UAS-Rac1*^{WT}/*genomic-dglurIIA*^{E783A}), and (S) *iGluR*^{MUT} + UAS-Rac1^{Act} (*dglurIIA*$^{Hypo/-}$,*IIB*$^{Df/-}$,*OK319-Gal4*;*UAS-Rac1*^{V12}/*genomic-dglurIIA*^{E783A}).

(D, E, M, N, T, and U) Quantification of the NMJ (D, M, and T) synaptic terminal area and (E, N, and U) bouton size index ($n \geq 23$) of the indicated genotypes normalized to controls (CS for *trio*$^{-/-}$ and *trio*$^{-/-}$ + UAS-Trio), (*cpx*$^{Df/+}$ for *cpx*$^{-/-}$ and *trio*$^{-/-}$;*cpx*$^{-/-}$ mutants), (*iGluR*^{WT} for *iGluR*^{MUT}).

Scale is the same in (A)–(C), in (F)–(H), in (I)–(S), in the insets of (I)–(L), and in the insets of (O)–(S). Error bars indicate ±SEM. *$p < 0.05$, **$p < 0.01$, ***$p < 0.001$. See also Figure S8.

DISCUSSION

In vertebrates, initial synaptic assembly appears to occur normally in the absence of all vesicular neurotransmission (Verhage et al., 2000), though subsequent aspects of structural development at some synapses are perturbed (Kummer et al., 2006; Witzemann et al., 2013). Similarly, we have found that depletion of both evoked and miniature NT disrupts *Drosophila* synaptic terminal development, particularly of the size of individual synaptic boutons. Surprisingly, however, we found that the specific abolishment of evoked NT using two different transgenic toxins had no effect on synaptic morphology. In contrast, synaptic development was disrupted when miniature NT was specifically depleted by manipulation of postsynaptic glutamate receptors. These phenotypes could be rescued by wild-type receptors, including mammalian glutamate receptors, but were unaltered by manipulating evoked NT. Oppositely, we found that increasing miniature NT is sufficient to induce synaptic terminal overgrowth. Using live imaging, we observed that enlargement of synaptic boutons is bidirectionally responsive to changes in miniature NT, and we found that this process was coupled with the ultrastructural maturation of synaptic active zones. We determined that miniature NT acts locally at synaptic terminals to regulate bouton maturation via a Trio GEF and Rac1 GTPase molecular signaling pathway. Our data therefore reveal a unique and specific requirement for miniature events in the development of synaptic terminals that is not shared with and cannot be compensated by evoked NT. These results indicate that

miniature neurotransmission, often dismissed as superfluous "noise" from evoked release, has essential and independent functions in vivo in the nervous system.

Miniature Neurotransmission Is Uniquely Required for Synapse Development

Our data reveal a surprisingly distinct requirement for miniature NT for normal synaptic development. Like many chemical synapses, the majority of neurotransmitter released at *Drosophila* NMJ terminals is via evoked NT. Not only is the amplitude of eEPSPs approximately 50-fold larger than mEPSPs at this terminal, but also evoked release occurs during endogenous activity as frequent rhythmic bursts (Kurdyak et al., 1994). Despite this, when evoked NT was completely abolished at these terminals, we observed no defects in morphological development, consistent with other studies (Dickman et al., 2006). Dissection of miniature NT from evoked release was made possible by exploiting synaptic homeostasis (Davis, 2013; Petersen et al., 1997), which we show occurs throughout the development of this terminal when postsynaptic glutamate receptors (iGluRs) are inhibited. Replacement of endogenous iGluRs by mutant subunits resulted in conditions where evoked NT was similar to controls, due to a relative increase in the number of synaptic vesicles released per action potential, but miniature NT was dramatically decreased. In these mutants, where miniature NT is depleted far more severely than in previous reports (e.g., dGluRIIA mutants; Petersen et al., 1997; data not shown), synaptic maturation was specifically perturbed. These defects were not reliant upon the activation of synaptic homeostasis because they were unaffected by manipulation of CamKII (Haghighi et al., 2003). Furthermore, very similar defects in synaptic development occur when presynaptic miniature neurotransmitter release is diminished by *vglut* mutations. Therefore, inhibition of the production or detection of postsynaptic miniature events results in developmental defects consistent with a transsynaptic signal. Moreover, additionally increasing or decreasing evoked release, when miniature NT is depleted, does not further alter synaptic development. In contrast, restoring miniature NT in iGluR mutants with either *Drosophila* or mammalian receptors can rescue normal terminal morphology. These results indicate that it is the discrete contribution of miniature NT rather than the total quantity of vesicular NT that is the critical factor necessary for normal synapse development. Therefore, the role of small miniature events during synapse development is qualitatively rather than quantitatively different from the function of larger evoked events. Miniature neurotransmission thus seems to act as a parallel second layer of synaptic communication with a unique and essential role in promoting normal synaptic structural development.

Synapse Maturation Requires Miniature Neurotransmission

Depletion of miniature NT results in terminals with aberrantly large numbers of small boutons. Two lines of evidence suggest that these small boutons are stalled in an immature phase of a normal growth process. First, live imaging revealed that when miniature NT is depleted, new boutons form at normal frequency but then fail to subsequently expand, unlike wild-type boutons. Second, small boutons in miniature NT mutants have synapse marker and ultrastructure features that appear identical to the small boutons of wild-type animals. These stalled boutons appear different from the aberrant small "satellite boutons" that occur when endocytosis is disrupted and have different synaptic marker and ultrastructure characteristics to normal boutons (Dickman et al., 2006). Therefore, our data support that miniature NT is critical for the normal progression of synaptic maturation. Since miniature NT is also a component of synaptic activity, it is intriguing to speculate that miniature events could contribute activity-dependent synaptic structural plasticity.

Localized Signaling by Miniature Neurotransmission

The discrete effect of altering miniature NT on individual bouton maturation coupled with the spatially restricted nature of these small events suggested a localized signaling activity. This was supported by our demonstration that miniature NT can regulate the development of individual synaptic terminals within a single neuron independently of each other. Interestingly, in cultured mammalian neurons, that activity of miniature NT on synaptic scaling also acts the levels of individual dendritic branches (Sutton et al., 2006), consistent with localized molecular signaling induced by miniature events in both paradigms. In *Drosophila*, we have identified Trio and Rac1 as essential components of the miniature NT signaling mechanism. *trio* mutants perturb synapse maturation in a manner similar to loss of miniature events, and activation of Trio or Rac1 can rescue miniature NT mutants. Trio and Rac1 have been implicated in actin dynamics in multiple contexts, including axonal growth cones and synapses (Ball et al., 2010; Miller et al., 2013), and GTPases can act as spatially confined "switches" inducing local cytoskeletal rearrangements. Interestingly, Trio is also transcriptionally regulated by the synaptotrophic BMP pathway (Ball et al., 2010) offering a potential molecular "node" to integrate local fine-tuning of maturation by miniature NT with global synaptic growth regulation. While our data support that Trio and Rac1 mediate the effects of miniature NT on presynaptic neurons, multiple intercellular signaling molecules can interact with Trio (Miller et al., 2013), requiring further investigation to establish how postsynaptic miniature events interact with this presynaptic pathway.

Discriminating between Miniature and Evoked Neurotransmission

Our studies beg the question of how miniature NT can be differentiated from evoked NT. The effects of miniature NT on developing synaptic boutons are both specific and localized. In mammalian cultured neurons, it has been suggested that miniature NT can target populations of postsynaptic receptors spatially separated to those activated by evoked neurotransmitter release (Ramirez and Kavalali, 2011). Consistent with this, it has also been directly observed that subpopulations of active zones at *Drosophila* synapses are specialized for the release of either miniature or evoked events (Melom et al., 2013; Peled et al., 2014). Therefore, miniature and evoked NT may activate spatially distinct postsynaptic signaling mechanisms. An alternative possibility is that differences in the release

kinetics between evoked and miniature NT could allow postsynaptic mechanisms to detect and differentiate between them. For example, local or global Ca^{2+} signaling through voltage-gated Ca^{2+} channels can be distinguished by calmodulin (Tadross et al., 2008). Unsynchronized activation of glutamate receptors through miniature events could also trigger downstream signaling mechanisms that are not activated by the synchronized activation of receptors by evoked release.

Reconsideration of Minis

In the past, miniature events were often dismissed as synaptic epiphenomena related to the requirement for a high fidelity of synaptic vesicle release during evoked NT (Sutton and Schuman, 2009; Zucker, 2005). Several studies over the last decade, however, have challenged this view. For example, miniature synaptic vesicle release has recently been found to be regulated by specialized Ca^{2+} sensors (Walter et al., 2011). mEPSPs can influence the firing rates of cerebellar interneurons, affect synaptic homeostasis, and at elevated levels trigger spiking of hippocampal neurons (Frank et al., 2006; Otsu and Murphy, 2003; Sutton and Schuman, 2009). In cultured neurons, miniature NT can stabilize spine structure and influence the activity of postsynaptic CamKII and is required for synaptic facilitation (Jin et al., 2012; Otsu and Murphy, 2003). Miniature NT can also alter local protein translation in dendrites and has been recently implicated as a potential mechanism of action of some fast-acting antidepressants (Kavalali and Monteggia, 2012; Sutton et al., 2006). Our data now demonstrate an in vivo role for miniature neurotransmission in the regulation of synapse development. Therefore, miniature events, a universal but often-overlooked feature of all chemical synapses, may be critical for many aspects of brain development and function.

EXPERIMENTAL PROCEDURES

See also Supplemental Experimental Procedures.

Drosophila Stocks

Motor neuron Gal4 drivers were OK319-Gal4 (Beck et al., 2012), OK6-Gal4 (Aberle et al., 2002), or D42-Gal4 (Yeh et al., 1995). Muscle Gal4 drivers were G14-Gal4 (Aberle et al., 2002), C57-Gal4 (Budnik et al., 1996), or H94-Gal4 (Davis and Goodman, 1998). Further details and descriptions of transgenic lines, mutant combinations, and transgenes are described in Supplemental Experimental Procedures.

Electrophysiology

Intracellular recordings were performed as previously described (McCabe et al., 2003) at physiological Ca^{2+} conditions (1.5 mM). eEPSP and mEPSP amplitudes, frequencies, and integrals were measured using the peak detection feature of the MiniAnalysis program (Synaptosoft). All events were verified manually while blinded to genotype. The amplitude, frequency, and integrals of mEPSPs were calculated from continuous recordings in the absence of stimulation (50–100 s). For animals expressing UAS-δACTX, unstimulated spontaneous multiquantal events occurred (data not shown), so mEPSP amplitude, frequency, and integrals were measured in the presence of tetrodotoxin (TTX) (4 μM final concentration), which did not affect miniature NT in control conditions. In *cpx* mutants, mEPSPs were so frequent that conventional measurements of frequency and amplitude were precluded, and the insect ionotropic glutamate receptor antagonist Philanthatoxin-343 (PhTox, Sigma) (Frank et al., 2006) was employed to establish the RMP baseline (4 μM final concentration).

Immunohistochemistry

Third-instar larvae of comparable size at the ~2 hr wandering stage time window were collected, dissected, and stained as previously described (McCabe et al., 2003). See Supplemental Experimental Procedures for details of the antibodies employed.

Morphological Analysis

All morphological analysis was done in maximum projections of z stacks from confocal images (Zeiss) of muscle 4 (Figures 1, 2, 3, 4, and 8) or muscles 6 and 7 (Figure 7) of segment A3, type Ib terminals only, identified by Dlg staining. All quantifications were performed while blinded to genotype. Synaptic terminal area was measured as the area of HRP-labeled presynaptic membrane surrounded by Dlg using MetaMorph (Molecular Devices). Typical boutons were counted as type Ib synaptic axonal varicosities with a size of >2 μm^2. Small boutons were counted as type Ib small (<2 μm^2) boutons labeled by Dlg. We restricted our analysis to small boutons that were clearly discernable. This may underestimate the actual number of small boutons, because small boutons partially occluded by surrounding typical boutons were excluded. The bouton size index was calculated by dividing the number of small boutons by the number of typical boutons per terminal.

Time-Lapse Live Imaging

Presynaptic motor neurons were labeled with membrane localized LexOp-CD8-GFP expressed by vglut-LexA (Baek et al., 2013) in both control and mutant backgrounds. Only images from animals that survived the entire 4-day imaging procedure were included in analysis. For bouton size expansion in live images, the size of each bouton was measured using the round regional tool of MetaMorph while blinded to genotype. Further details are in Supplemental Experimental Procedures.

Electron Microscopy

Electron microscopy and ultrastructure quantification were previously described (Jiao et al., 2010). Only type Ib boutons, identified by postsynaptic subsynaptic reticulum structure, were selected for quantification. Small boutons were defined as having the longest axis among serial section <1.6 μm, based on a 2-dimensional projection area of <2 μm^2. All small boutons were identified using serial sections. Frequency of T-bar per active zone was verified by serial section images around the active zone. T-bar size was measured at middle images of serial sections where the T-bar size was largest.

Data Analysis

Statistical significance for all morphological and electrophysiological data were determined using a Kruskal-Wallis test followed by a Dunn's post hoc test when multiple comparisons were required. Otherwise, we employed Mann-Whitney-Wilcoxon test (Instat, GraphPad) except for Figures 6E and S6J, where Fisher's exact test was used.

SUPPLEMENTAL INFORMATION

Supplemental Information includes Supplemental Experimental Procedures, eight figures, and one table and can be found with this article online at http://dx.doi.org/10.1016/j.neuron.2014.03.012.

ACKNOWLEDGMENTS

We are grateful to Rafael Yuste, Amy McDermott, George Mentis, and Erin Beck for critical reading of the manuscript. We thank Stephan Sigrist, Aaron DiAntonio, Troy Littleton, Fumiko Kawasaki, Hermann Aberle, Pejmun Haghighi, Cahir O'Kane, Rachel Kraut, Vivian Budnik, Richard Mann, Corey Goodman, Robert Oswald, and the Bloomington and the Vienna stock centers for stocks, advice, and reagents. We thank Tim Crawley, Liyan McCurdy, and Mitchell Hayes for technical assistance. B.J.C. was supported by NIH 5T32HL08774, and Y.W. was supported by F32NS055527. Work in the laboratory of R.A.B. is funded by the Wellcome Trust (090798/Z/09/Z). Work in the laboratory of M.N.N. is funded by NIH NS055035, NS056443, NS058330, and GM098931. Work in the laboratory of B.D.M. was supported by NIH

NS075572, AG08702, the DANA foundation, the Gatsby Initiative in brain circuitry and the New York Presbyterian Seizure Disorders Fund.

Accepted: February 18, 2014
Published: May 7, 2014

REFERENCES

Aberle, H., Haghighi, A.P., Fetter, R.D., McCabe, B.D., Magalhães, T.R., and Goodman, C.S. (2002). wishful thinking encodes a BMP type II receptor that regulates synaptic growth in Drosophila. Neuron *33*, 545–558.

Baek, M., Enriquez, J., and Mann, R.S. (2013). Dual role for Hox genes and Hox co-factors in conferring leg motoneuron survival and identity in Drosophila. Development *140*, 2027–2038.

Ball, R.W., Warren-Paquin, M., Tsurudome, K., Liao, E.H., Elazzouzi, F., Cavanagh, C., An, B.-S., Wang, T.-T., White, J.H., and Haghighi, A.P. (2010). Retrograde BMP signaling controls synaptic growth at the NMJ by regulating trio expression in motor neurons. Neuron *66*, 536–549.

Beck, E.S., Gasque, G., Imlach, W.L., Jiao, W., Jiwon Choi, B., Wu, P.-S., Kraushar, M.L., and McCabe, B.D. (2012). Regulation of Fasciclin II and synaptic terminal development by the splicing factor beag. J. Neurosci. *32*, 7058–7073.

Brose, N. (2008). For better or for worse: complexins regulate SNARE function and vesicle fusion. Traffic *9*, 1403–1413.

Budnik, V., Koh, Y.H., Guan, B., Hartmann, B., Hough, C., Woods, D., and Gorczyca, M. (1996). Regulation of synapse structure and function by the Drosophila tumor suppressor gene dlg. Neuron *17*, 627–640.

Collins, C.A., and DiAntonio, A. (2007). Synaptic development: insights from Drosophila. Curr. Opin. Neurobiol. *17*, 35–42.

Daniels, R.W., Collins, C.A., Chen, K., Gelfand, M.V., Featherstone, D.E., and DiAntonio, A. (2006). A single vesicular glutamate transporter is sufficient to fill a synaptic vesicle. Neuron *49*, 11–16.

Davis, G.W. (2013). Homeostatic signaling and the stabilization of neural function. Neuron *80*, 718–728.

Davis, G.W., and Goodman, C.S. (1998). Synapse-specific control of synaptic efficacy at the terminals of a single neuron. Nature *392*, 82–86.

Dickman, D.K., Lu, Z., Meinertzhagen, I.A., and Schwarz, T.L. (2006). Altered synaptic development and active zone spacing in endocytosis mutants. Curr. Biol. *16*, 591–598.

Egebjerg, J., Bettler, B., Hermans-Borgmeyer, I., and Heinemann, S. (1991). Cloning of a cDNA for a glutamate receptor subunit activated by kainate but not AMPA. Nature *351*, 745–748.

Fatt, P., and Katz, B. (1952). Spontaneous subthreshold activity at motor nerve endings. J. Physiol. *117*, 109–128.

Frank, C.A., Kennedy, M.J., Goold, C.P., Marek, K.W., and Davis, G.W. (2006). Mechanisms underlying the rapid induction and sustained expression of synaptic homeostasis. Neuron *52*, 663–677.

Haghighi, A.P., McCabe, B.D., Fetter, R.D., Palmer, J.E., Hom, S., and Goodman, C.S. (2003). Retrograde control of synaptic transmission by postsynaptic CaMKII at the Drosophila neuromuscular junction. Neuron *39*, 255–267.

Hoang, B., and Chiba, A. (2001). Single-cell analysis of Drosophila larval neuromuscular synapses. Dev. Biol. *229*, 55–70.

Huntwork, S., and Littleton, J.T. (2007). A complexin fusion clamp regulates spontaneous neurotransmitter release and synaptic growth. Nat. Neurosci. *10*, 1235–1237.

Iyer, J., Wahlmark, C.J., Kuser-Ahnert, G.A., and Kawasaki, F. (2013). Molecular mechanisms of COMPLEXIN fusion clamp function in synaptic exocytosis revealed in a new Drosophila mutant. Mol. Cell. Neurosci. *56*, 244–254.

Jiao, W., Shupliakov, A., and Shupliakov, O. (2010). A semi-correlative technique for the subcellular localization of proteins in Drosophila synapses. J. Neurosci. Methods *185*, 273–279.

Jin, I., Puthanveettil, S., Udo, H., Karl, K., Kandel, E.R., and Hawkins, R.D. (2012). Spontaneous transmitter release is critical for the induction of long-term and intermediate-term facilitation in Aplysia. Proc. Natl. Acad. Sci. USA *109*, 9131–9136.

Kauwe, G., and Isacoff, E.Y. (2013). Rapid feedback regulation of synaptic efficacy during high-frequency activity at the Drosophila larval neuromuscular junction. Proc. Natl. Acad. Sci. USA *110*, 9142–9147.

Kavalali, E.T., and Monteggia, L.M. (2012). Synaptic mechanisms underlying rapid antidepressant action of ketamine. Am. J. Psychiatry *169*, 1150–1156.

Kittel, R.J., Wichmann, C., Rasse, T.M., Fouquet, W., Schmidt, M., Schmid, A., Wagh, D.A., Pawlu, C., Kellner, R.R., Willig, K.I., et al. (2006). Bruchpilot promotes active zone assembly, Ca2+ channel clustering, and vesicle release. Science *312*, 1051–1054.

Koch, I., Schwarz, H., Beuchle, D., Goellner, B., Langegger, M., and Aberle, H. (2008). Drosophila ankyrin 2 is required for synaptic stability. Neuron *58*, 210–222.

Kummer, T.T., Misgeld, T., and Sanes, J.R. (2006). Assembly of the postsynaptic membrane at the neuromuscular junction: paradigm lost. Curr. Opin. Neurobiol. *16*, 74–82.

Kurdyak, P., Atwood, H.L., Stewart, B.A., and Wu, C.F. (1994). Differential physiology and morphology of motor axons to ventral longitudinal muscles in larval Drosophila. J. Comp. Neurol. *350*, 463–472.

Mahr, A., and Aberle, H. (2006). The expression pattern of the Drosophila vesicular glutamate transporter: a marker protein for motoneurons and glutamatergic centers in the brain. Gene Expr. Patterns *6*, 299–309.

McCabe, B.D., Marqués, G., Haghighi, A.P., Fetter, R.D., Crotty, M.L., Haerry, T.E., Goodman, C.S., and O'Connor, M.B. (2003). The BMP homolog Gbb provides a retrograde signal that regulates synaptic growth at the Drosophila neuromuscular junction. Neuron *39*, 241–254.

Melom, J.E., Akbergenova, Y., Gavornik, J.P., and Littleton, J.T. (2013). Spontaneous and evoked release are independently regulated at individual active zones. J. Neurosci. *33*, 17253–17263.

Miller, M.B., Yan, Y., Eipper, B.A., and Mains, R.E. (2013). Neuronal Rho GEFs in synaptic physiology and behavior. Neuroscientist *19*, 255–273.

Otsu, Y., and Murphy, T.H. (2003). Miniature transmitter release: accident of nature or careful design? Sci. STKE *2003*, pe54.

Peled, E.S., Newman, Z.L., and Isacoff, E.Y. (2014). Evoked and spontaneous transmission favored by distinct sets of synapses. Curr. Biol. *24*, 484–493.

Petersen, S.A., Fetter, R.D., Noordermeer, J.N., Goodman, C.S., and DiAntonio, A. (1997). Genetic analysis of glutamate receptors in Drosophila reveals a retrograde signal regulating presynaptic transmitter release. Neuron *19*, 1237–1248.

Ramirez, D.M.O., and Kavalali, E.T. (2011). Differential regulation of spontaneous and evoked neurotransmitter release at central synapses. Curr. Opin. Neurobiol. *21*, 275–282.

Schmid, A., Qin, G., Wichmann, C., Kittel, R.J., Mertel, S., Fouquet, W., Schmidt, M., Heckmann, M., and Sigrist, S.J. (2006). Non-NMDA-type glutamate receptors are essential for maturation but not for initial assembly of synapses at Drosophila neuromuscular junctions. J. Neurosci. *26*, 11267–11277.

Schuster, C.M., Davis, G.W., Fetter, R.D., and Goodman, C.S. (1996). Genetic dissection of structural and functional components of synaptic plasticity. I. Fasciclin II controls synaptic stabilization and growth. Neuron *17*, 641–654.

Stuart, G., and Sakmann, B. (1995). Amplification of EPSPs by axosomatic sodium channels in neocortical pyramidal neurons. Neuron *15*, 1065–1076.

Sutton, M.A., and Schuman, E.M. (2009). Partitioning the synaptic landscape: distinct microdomains for spontaneous and spike-triggered neurotransmission. Sci. Signal. *2*, pe19.

Sutton, M.A., Ito, H.T., Cressy, P., Kempf, C., Woo, J.C., and Schuman, E.M. (2006). Miniature neurotransmission stabilizes synaptic function via tonic suppression of local dendritic protein synthesis. Cell *125*, 785–799.

Sweeney, S.T., Broadie, K., Keane, J., Niemann, H., and O'Kane, C.J. (1995). Targeted expression of tetanus toxin light chain in Drosophila specifically eliminates synaptic transmission and causes behavioral defects. Neuron *14*, 341–351.

Tadross, M.R., Dick, I.E., and Yue, D.T. (2008). Mechanism of local and global Ca2+ sensing by calmodulin in complex with a Ca2+ channel. Cell *133*, 1228–1240.

Turrigiano, G. (2012). Homeostatic synaptic plasticity: local and global mechanisms for stabilizing neuronal function. Cold Spring Harb. Perspect. Biol. *4*, a005736.

Ueda, A., and Kidokoro, Y. (1996). Longitudinal body wall muscles are electrically coupled across the segmental boundary in the third instar larva of Drosophila melanogaster. Invert. Neurosci. *1*, 315–322.

Verhage, M., Maia, A.S., Plomp, J.J., Brussaard, A.B., Heeroma, J.H., Vermeer, H., Toonen, R.F., Hammer, R.E., van den Berg, T.K., Missler, M., et al. (2000). Synaptic assembly of the brain in the absence of neurotransmitter secretion. Science *287*, 864–869.

Walter, A.M., Groffen, A.J., Sørensen, J.B., and Verhage, M. (2011). Multiple Ca2+ sensors in secretion: teammates, competitors or autocrats? Trends Neurosci. *34*, 487–497.

Witzemann, V., Chevessier, F., Pacifici, P.G., and Yampolsky, P. (2013). The neuromuscular junction: selective remodeling of synaptic regulators at the nerve/muscle interface. Mech. Dev. *130*, 402–411.

Wu, Y., Cao, G., Pavlicek, B., Luo, X., and Nitabach, M.N. (2008). Phase coupling of a circadian neuropeptide with rest/activity rhythms detected using a membrane-tethered spider toxin. PLoS Biol. *6*, e273.

Yeh, E., Gustafson, K., and Boulianne, G.L. (1995). Green fluorescent protein as a vital marker and reporter of gene expression in Drosophila. Proc. Natl. Acad. Sci. USA *92*, 7036–7040.

Zito, K., Parnas, D., Fetter, R.D., Isacoff, E.Y., and Goodman, C.S. (1999). Watching a synapse grow: noninvasive confocal imaging of synaptic growth in Drosophila. Neuron *22*, 719–729.

Zucker, R.S. (2005). Minis: whence and wherefore? Neuron *45*, 482–484.

Neuron, Volume *82*

Supplemental Information

Miniature Neurotransmission Regulates *Drosophila* Synaptic Structural Maturation

Ben Jiwon Choi, Wendy L. Imlach, Wei Jiao, Verena Wolfram, Ying Wu, Mark Grbic, Carolina Cela, Richard A. Baines, Michael N. Nitabach, and Brian D. McCabe

Abbreviation	Genotype	N #	Control	Synaptic Terminal Area (μm^2) (Significance vs Control)	Number of typical synaptic bouton (number) (Significance vs Control)	Number of small synaptic bouton (number) (Significance vs Control)	Bouton size index (number) (Significance vs Control)
Control(toxin) CS	CantonS	48	**N/A**	292.4±7.976	24.000±0.672	2.878±0.301	0.1254±0.0146
UAS-TeTxLC	UAS-TeTxLC/*OK319-Gal4*	54	**CS**	300.09±8.574 (ns)	24.056±0.690 (ns)	3.333±0.400 (ns)	0.1511±0.0205 (ns)
UAS-PLTXII	*OK6- Gal4/+;+/UAS-PLTXII*	39	**CS**	301.84±7.674 (ns)	23.556±0.537 (ns)	2.143±0.229 (ns)	0.0921±0.0111 (ns)
Control(*vglut*) *vglut*$^{Df/+}$	*Vglut*$^{OK371\Delta D}$/+	37	**N/A**	347.79±8.283	34.162±0.857	4.000±0.365	0.1215±0.0125
***vglut*^{MN}**	*vglut*^{1}/*vglut*$^{OK371\Delta D}$,*UAS-Vglut-RNAi*^{JF02689};*D42-Gal4/UAS-Vglut-RNAi*^{VDRC104324}	30	***vglut*$^{Df/+}$**	263.02±8.734 (***)	22.967±0.702 (***)	9.433±0.974 (***)	0.4447±0.0543 (***)
Vglut-RNAi#1	*UAS-Vglut-RNAi*^{VDRC104324}/+; *UAS-Vglut-RNAi*^{JF02689}/*D42-Gal4*	33	**CS**	271.09±4.996 (*)	21.879±0.701 (*)	5.827±0.665 (***)	0.2508±0.0340 (**)
Vglut-RNAi#2	*OK6-Gal4/+;D42-Gal4/UAS-Vglut-RNAi*^{HMS02011}	32	**CS**	263.65±8.578 (*)	20.000±0.743 (***)	6.281±0.570 (***)	0.3426±0.0382 (***)
***vglut*^{Hypo}**	*vglut*^{1}/*vglut*$^{OK371\Delta D}$	48	***vglut*$^{Df/+}$**	302.21±4.204 (***)	27.021±0.633 (***)	6.292±0.478 (**)	0.2368±0.0182 (***)
***vglut*^{Hypo} + UAS-Vglut**	*vglut*^{1},*OK319-Gal4/vglut*$^{OK371\Delta D}$;*+/UAS-Vglut*	24	***vglut*$^{Df/+}$**	359.34±20.947 (ns)	30.435±1.002 (**)	3.150±0.399 (ns)	0.0905±0.0134 (ns)
Control (Fig.2) *dgluRIIA*$^{+/-}$,*IIB*$^{Df/-}$	*dglurIIA,IIB*^{sp22}/ *Df(2L)cl*^{h4} ; *genomic-dglurIIA/+*	44	**N/A**	302.83±6.05	32.886±0.927	2.136±0.267	0.06784±0.0091
***dgluRIIA*$^{Hypo/-}$,*IIB*$^{Df/-}$**	*dglurIIA,IIB*^{sp22}/ *Df(2L)cl*^{h4}, *genomic-dglurIIAΔ3UTR*						
***iGluR*^{WT}**	*dglurIIA,IIB*^{sp22}/ *Df(2L)cl*^{h4}, *genomic-dglurIIA*Δ3UTR; *genomic-dglurIIA*^{WT}/+	59	***dgluRIIA*$^{+/-}$,*IIB*$^{Df/-}$**	318.25±6.910 (ns)	30.862±0.683 (ns)	2.259±0.253 (ns)	0.07391±0.00864 (ns)
***iGluR*^{MUT}**	*dglurIIA,IIB*^{sp22}/ *Df(2L)cl*^{h4}, *genomic-dglurIIA*Δ3UTR; *genomic-dglurIIA*^{E783A}/+	53	***dgluRIIA*$^{+/-}$,*IIB*$^{Df/-}$ (Fig. 2) *iGluR*^{WT} (Fig. 3,5,7,8)**	231.12±7.906 (***)	19.850±0.843 (***)	6.025±0.541 (***)	0.3272±0.0330 (***)
***iGluR*^{MUT} + UAS-dGluR^{WT}**	*dglurIIA,IIB*^{sp22},*G14-Gal4/ Df(2L)cl*^{h4}, *genomic-dglurIIA*Δ3UTR; *genomic-dglurIIA*^{E783A}/*UAS-dglurIIA*	22	***dgluRIIA*$^{+/-}$,*IIB*$^{Df/-}$**	345.16±11.512 (***)	27.773±0.822 (**)	3.421±0.650 (ns)	0.1161±0.0298 (ns)
***iGluR*^{MUT} + UAS-CamKII^{Act}**	*dglurIIA,IIB*^{sp22},*G14-Gal4/ Df(2L)cl*^{h4}, *genomic-dglurIIA*Δ3UTR; *genomic-dglurIIA*^{E783A}/*UAS-CamKII*^{T287D}	17	***iGluR*^{WT}**	260.65±14.480 (**)	22.824±0.892 (***)	9.823±0.792 (***)	0.4483±0.0473 (***)
***iGluR*^{MUT} + UAS-CamKII^{Inh}**	*dglurIIA,IIB*^{sp22},*G14-Gal4/ Df(2L)cl*^{h4}, *genomic-dglurIIA*Δ3UTR; *genomic-dglurIIA*^{E783A}/*UAS-CamKIINtide*	19	***iGluR*^{WT}**	260.64±10.837 (***)	20.842±0.922 (***)	8.684±0.722 (***)	0.4377±0.0415 (***)
***iGluR*^{MUT} + UAS-PLTXII**	*dglurIIA,IIB*^{sp22},*OK319-Gal4/ Df(2L)cl*^{h4}, *genomic-dglurIIA*Δ3UTR; *genomic-dglurIIA*^{E783A}/*UAS-PLTXII*	36	***iGluR*^{WT}**	240.60±10.122 (***)	20.721±0.661 (***)	6.932±0.505 (***)	0.3276±0.0252 (***)
***iGluR*^{MUT} + UAS-δACTX**	*dglurIIA,IIB*^{sp22},*OK319-Gal4/ Df(2L)cl*^{h4}, *genomic-dglurIIA*Δ3UTR; *genomic-dglurIIA*^{E783A}/ *UAS-δACTX*	27	***iGluR*^{WT}**	252.36±14.182 (***)	21.96±1.194 (***)	6.231±0.939 (***)	0.2819±0.0423 (***)
***iGluR*^{MUT} + UAS-rGluK2**	*dglurIIA,B*^{sp22},*G14-Gal4/ Df(2L)cl*^{h4}, *genomic-dglurIIA*Δ3UTR; *genomic-dglurIIA*^{E783A}/ *UAS-rGluK2*	41	***iGluR*^{WT}**	331.91±6.168 (ns)	27.780±0.693 (**)	4.268±0.446 (***)	0.1553±0.01610 (***)
***iGluR*^{MUT} + UAS-rGluK2 + UAS-PLTXII**	*dglurIIA,IIB*^{sp22},*G14-Gal4,OK319-Gal4/ Df(2L)cl*^{h4}, *genomic-dglurIIA*Δ3UTR; *genomic-dglurIIA*^{E783A},*UAS-PLTXII/UAS-rGluK2*	34	***iGluR*^{WT}**	318.95±9.954 (ns)	27.647±0.736 (**)	4.206±0.372 (***)	0.1568±0.01447 (***)
UAS-PLTXII (muscle)	*G14-Gal4/+;+/UAS-PLTXII*	15	**CS**	305.66±15.387 (ns)	26.667±1.120 (ns)	4.142±0.592 (*)	0.1505±0.02657 (ns)

Table S1

UAS-rGluK2 (neuron)	*OK319-Gal4/+;+/UAS-rGluK2*	16	**CS**	308.34±13.395 (ns)	24.125±0.645 (ns)	2.231±0.441 (ns)	0.07540±0.01777 (ns)
***vglut*^{Hypo} + UAS-PLTXII**	*vglut*^{1},*OK319-Gal4/vglut* $^{OK371\Delta D}$*;+/UAS-PLTXII*	26	***vglut*$^{Df/+}$**	298.85±7.872 (***)	25.308±0.658 (***)	6.731±0.890 (*)	0.2825±0.04470 (***)
***vglut*^{Hypo} + UAS-δACTX**	*vglut*^{1},*OK319-Gal4/vglut* $^{OK371\Delta D}$*;+/UAS- δACTX*	25	***vglut*$^{Df/+}$**	288.72±13.379 (**)	25.520±1.022 (***)	6.760±0.710 (**)	0.2705±0.03107 (***)
Control(*cpx*) *cpx*$^{Df/+}$	*Df(3R)ED5021/+*	35	**N/A**	282.98±6.927	25.694±0.720	3.556±0.426	0.1407±0.0163
***cpx*$^{-/-}$**	*Df(3R)ED5021/cpx*^{SH1}	38	***cpx*$^{Df/+}$**	407.96±11.755 (***)	33.795±1.068 (***)	1.897±0.276 (**)	0.0598±0.00902 (***)
***cpx*$^{-/-}$ + UAS-Cpx**	*UAS-Cpx/+;OK6-Gal4/+;Df(3R)ED5021/cpx*^{SH1}	46	***cpx*$^{Df/+}$**	312.79±8.318 (ns)	28.067±0.853 (ns)	4.933±0.433 (*)	0.1863±0.0172 (ns)
***Cpx*$^{1257/-}$**	*Df(3R)ED5021/cpx*^{1257}	23	***cpx*$^{Df/+}$**	432.33±26.326 (***)	33.65±0.8331 (***)	3.182±0.439 (ns)	0.08891±0.0136 (*)
***cpx*$^{-/-}$ + UAS-PLTXII**	*OK6-Gal4/UAS-PLTXII;Df(3R)ED5021/cpx*^{SH1}	24	***cpx*$^{Df/+}$**	391.62±10.172 (***)	35.50±1.234 (***)	1.292±0.321 (***)	0.03705±0.00896 (***)
***cpx*$^{-/-}$ + UAS-dGluR^{DN}**	*G14-Gal4/UAS-dglurIIA*^{E783A}*;Df(3R)ED5021/ cpx*^{SH1}	41	***cpx*$^{Df/+}$**	262.65±10.146 (ns)	25.105±0.951 (ns)	3.447±0.507 (ns)	0.1518±0.0289 (ns)
***cpx*$^{-/-}$ + Vglut-RNAi**	*OK6-Gal4/ UAS-Vglut-RNAi*^{VDRC104324}*;Df(3R)ED5021 /cpx*^{SH1}	56	***cpx*$^{Df/+}$**	333.78±7.394 (**)	28.585±0.839 (ns)	5.018±0.455 (*)	0.1881±0.0193 (*)
UAS-dGluR^{DN}	*G14-Gal4/UAS-dglurIIA*^{E783A}	29	**CS**	279.49±10.734 (ns)	25.964±0.864 (ns)	2.071±0.329 (*)	0.08391±0.0138 (*)
Vglut-RNAi	*OK6-Gal4/ UAS-Vglut-RNAi*^{VDRC104324}	28	**CS**	275.59±9.57 (ns)	26.034±1.318 (ns)	5.241±0.683 (***)	0.2152±0.0327 (***)
***trio*$^{-/-}$**	*trio*^{S137203}*/trio*^{S137203}	30	**CS**	192.81±8.794 (***)	17.194±0.905 (***)	5.700±0.526 (***)	0.3549±0.4404 (***)
***Trio*$^{-/-}$ + UAS-Trio**	*UAS-Trio/+;+/OK319-Gal4; trio*^{S137203}*/trio*^{S137203}	23	**CS**	291.98±12.734 (ns)	23.608±0.963 (ns)	2.545±0.3821 (ns)	0.09846±0.01471 (ns)
***trio*$^{-/-}$; *cpx*$^{-/-}$**	*trio*^{S137203}*/trio*^{S137203}*; cpx*^{SH1}*/cpx*^{SH1}	28	***cpx*$^{Df/+}$**	204.62±8.34 (***)	19.467±0.716 (***)	7.267±0.959 (**)	0.3893±0.0524 (***)
***iGluR*^{MUT} + UAS-Trio**	*dglurIIA,IIB*^{sp22}*,OK319-Gal4/ Df(2L)cl*^{h4}*, genomic-dglurIA*Δ3UTR*; genomic-dglurIA*^{E783A}*/UAS-Trio*	30	***iGluR*^{WT}**	305.37±14.7 (ns)	28.74±1.07 (ns)	5.345±0.659 (***)	0.1842±0.0253 (***)
***iGluR*^{MUT} + UAS-Rac1^{WT}**	*dglurIIA,IIB*^{sp22}*,OK319-Gal4/ Df(2L)cl*^{h4}*, genomic-dglurIA*Δ3UTR*; genomic-dglurIA*^{E783A}*/UAS-Rac1*	23	***iGluR*^{WT}**	256.03±16.41 (**)	22.09±1.17 (***)	5.909±0.916 (***)	0.3478±0.0620 (***)
***iGluR*^{MUT} + UAS-Rac1^{Act}**	*dglurIIA,IIB*^{sp22}*,OK319-Gal4/ Df(2L)cl*^{h4}*, genomic-dglurIA*Δ3UTR*; genomic-dglurIA*^{E783A}*/UAS-Rac1*^{V12}	23	***iGluR*^{WT}**	306.46±19.93 (ns)	30.2±0.846 (ns)	5.077±0.604 (***)	0.1482±0.0226 (**)
***iGluR*^{WT} + *trio*$^{-/-}$**	*dglurIIA,IIB*^{sp22}*/ Df(2L)cl*^{h4}*, genomic-dglurIA*Δ3UTR*; trio*^{S137203}*,genomic-dglurIA/ trio*^{S137203}	35	***iGluR*^{WT}**	180.53±7.62 (***)	11.861±0.524 (***)	4.297±0.525 (***)	0.4459±0.0814 (***)
***iGluR*^{MUT} + *trio*$^{-/-}$**	*dglurIIA,IIB*^{sp22}*/ Df(2L)cl*^{h4}*, genomic-dglurIA*Δ3UTR*; trio*^{S137203}*,genomic-dglurIA*^{E783A}*/ trio*^{S137203}	24	***iGluR*^{WT}**	188.25±7.93 (***)	13.125±0.588 (***)	6.960±0.488 (***)	0.5243±0.0343 (***)
***iGluR*^{WT} + UAS-Trio**	*dglurIIA,IIB*^{sp22}*,OK319-Gal4/ Df(2L)cl*^{h4}*, genomic-dglurIA*Δ3UTR*; genomic-dglurIA*^{WT}*/UAS-Trio*	26	***iGluR*^{WT}**	347.17±8.94 (*)	33.96±0.774 (**)	3.038±0.316 (ns)	0.089±0.01046 (ns)
***iGluR*^{WT} + UAS-Rac1^{WT}**	*dglurIIA,IIB*^{sp22}*,OK319-Gal4/ Df(2L)cl*^{h4}*, genomic-dglurIA*Δ3UTR*; genomic-dglurIA*^{WT}*/UAS-Rac1*^{WT}	32	***iGluR*^{WT}**	380.60±14.53 (***)	35.43±1.04 (***)	8.100±0.894 (***)	0.2301±0.02714 (***)
***iGluR*^{WT} + UAS-Rac1^{Act}**	*dglurIIA,IIB*^{sp22}*,OK319-Gal4/ Df(2L)cl*^{h4}*, genomic-dglurIA*Δ3UTR*; genomic-dglurIA*^{WT}*/UAS-Rac1*^{V12}	22	***iGluR*^{WT}**	316.51±12.74 (ns)	31.08±1.16 (ns)	4.208±0.430 (***)	0.1355±0.01251 (***)

Table S1 (Continued)

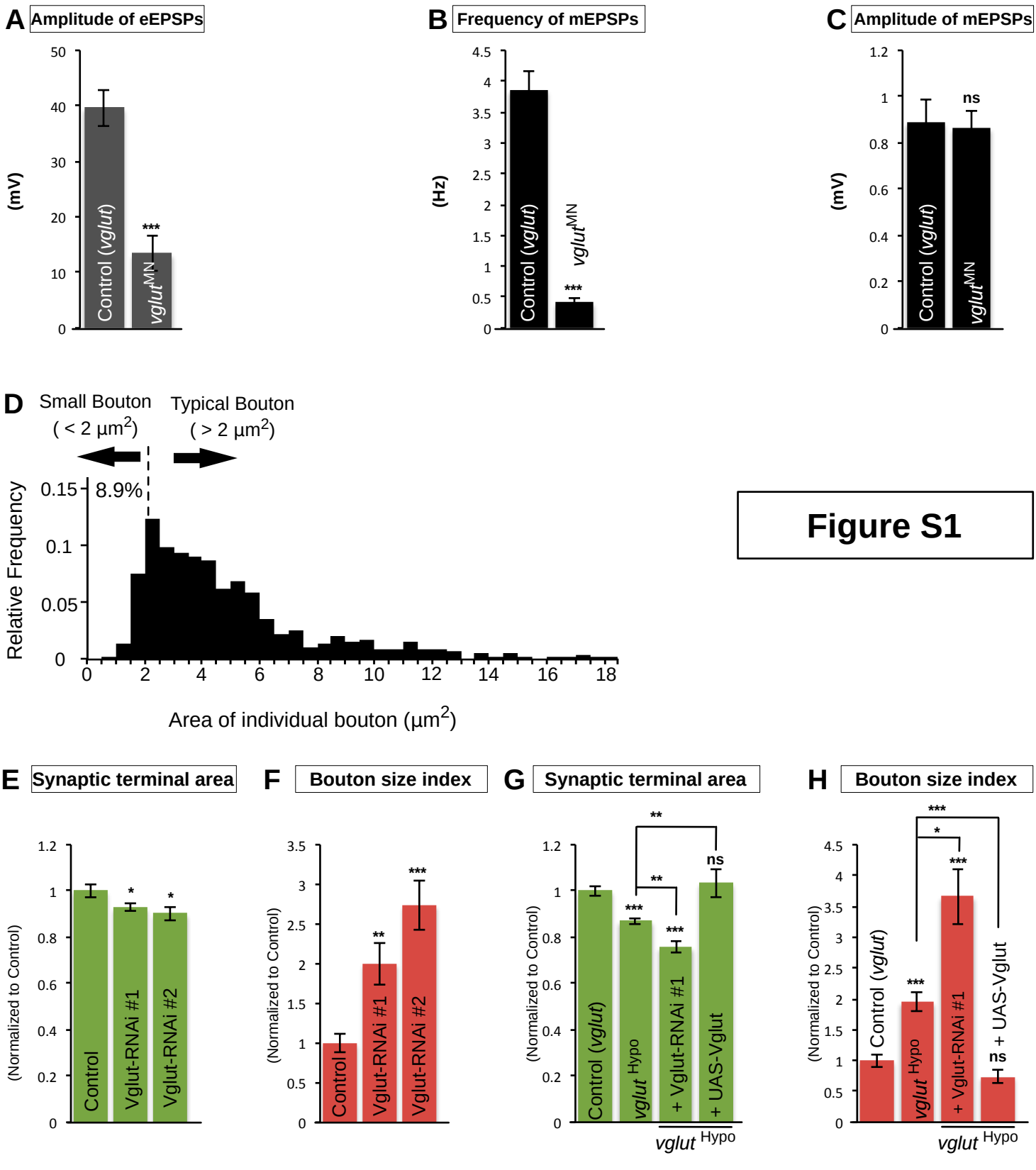

Figure S1

vglut MN = *vglut* Hypo + Vglut-RNAi #1

Figure S1. Electrophysiological and morphological quantification of *vglut* mutants and bouton size distribution of wild type terminals, Related to Figure 1.

A-C, Quantification of (A) the amplitude of eEPSPs (n≥6), (B) the frequency of mEPSPs and (C) the amplitude of mEPSPs (n≥9). **D,** Relative frequency histogram for the distribution of individual bouton sizes of wild type (CS) boutons in 0.5μm^2 increments. (n=603 boutons from n=16 NMJs) **E-H**, Quantification of the NMJ (E,G) synaptic terminal area and (F,H) bouton size index (n≥24) of the **Control** [CS], **Vglut1-RNAi#1** [*+/UAS-Vglut-RNAi*^{KK}*;D42-Gal4/UAS-Vglut-RNAi*^{JF}], **Vglut1-RNAi#2** [*OK6-Gal4/+;D42-Gal4/UAS-Vglut-RNAi*^{HMS}], **Control(*vglut*)** [*vglut*$^{Df/+}$], ***vglut*^{Hypo}** [*vglut*$^{Hypo/Df}$], ***vglut*^{Hypo} + Vglut-RNAi#1** [***vglut*^{MN}** = *vglut*$^{Hypo/Df}$,*UAS-Vglut-RNAi*^{KK}*;D42-Gal4/UAS-Vglut-RNAi* ^{JF}] and ***vglut*^{Hypo} + UAS-Vglut** [*vglut*$^{Hypo/Df}$,*OK319-Gal4;+/UAS-Vglut*] normalized to controls [CS for E,F and *vglut*$^{Df/+}$ for G,H] Error bars indicate ± s.e.m. *=p<0.05, **= p<0.01, ***=p< 0.001.

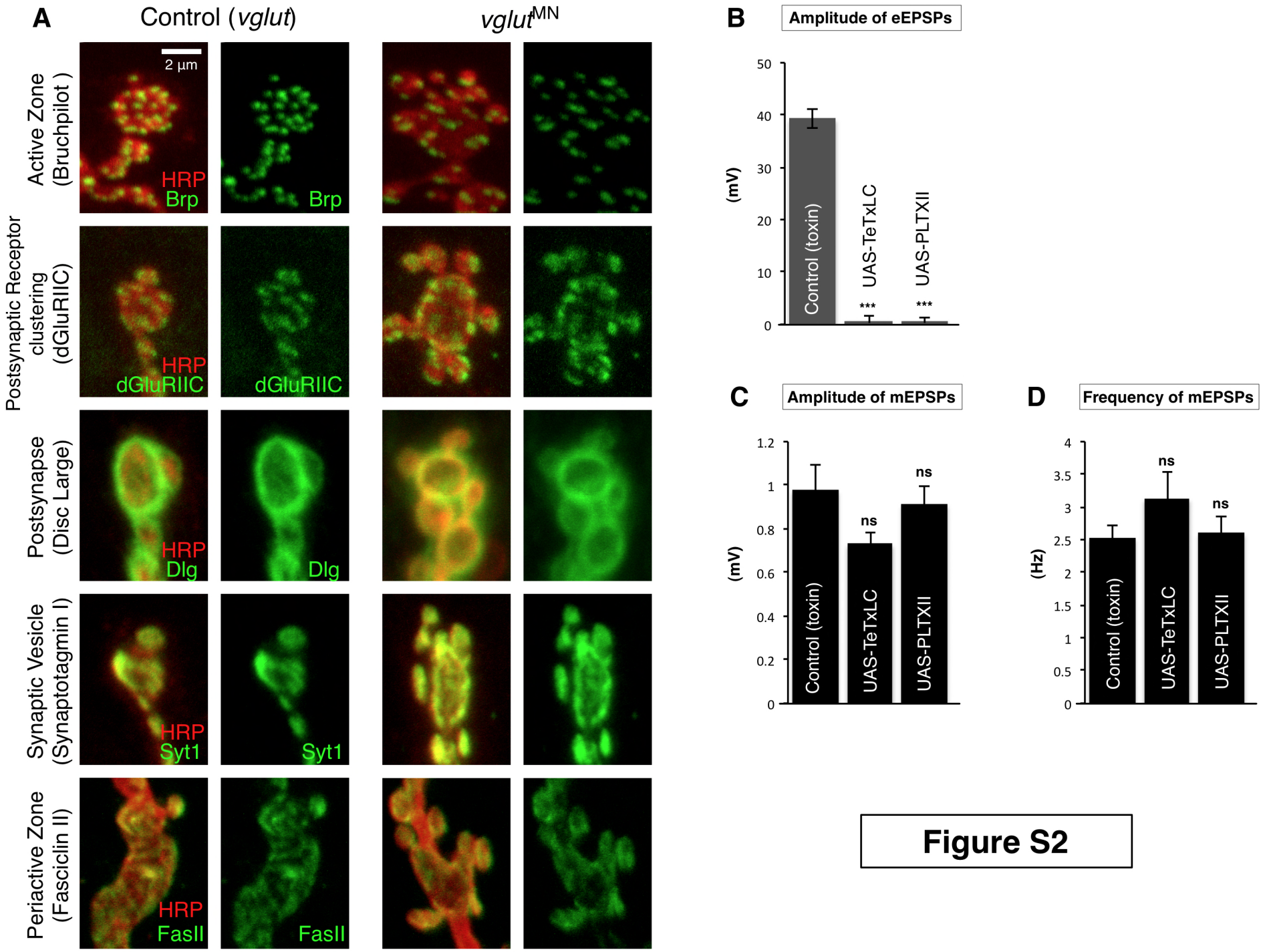
A
Control (vglut)
vglutMN
2 µm
Active Zone (Bruchpilot)
HRP Brp
Brp
Postsynaptic Receptor clustering (dGluRIIC)
HRP dGluRIIC
dGluRIIC
Postsynapse (Disc Large)
HRP Dlg
Dlg
Synaptic Vesicle (Synaptotagmin I)
HRP Syt1
Syt1
Periactive Zone (Fasciclin II)
HRP FasII
FasII
B
Amplitude of eEPSPs
(mV)
50
40
30
20
10
0
Control (toxin)
UAS-TeTxLC
UAS-PLTXII
***
***
C
Amplitude of mEPSPs
(mV)
1.2
1
0.8
0.6
0.4
0.2
0
Control (toxin)
UAS-TeTxLC
UAS-PLTXII
ns
ns
D
Frequency of mEPSPs
(Hz)
4
3.5
3
2.5
2
1.5
1
0.5
0
Control (toxin)
UAS-TeTxLC
UAS-PLTXII
ns
ns

Figure S2

Figure S2. Synaptic markers at small boutons of *vglut* mutants and electrophysiological quantification of toxin mutants, Related to Figure 1.

A, Representative boutons from control(*vglut*) [$vglut^{Df/+}$] and $vglut^{MN}$ at muscle 4 labeled with indicated synaptic markers (green) and the neuronal membrane marker HRP (red). Scale is the same for all images. **B-D**, Quantification of (B) the amplitude of eEPSPs ($n \geq 6$), (C) the amplitude of mEPSPs and (D) the frequency of mEPSPs ($n \geq 9$). All error bars indicate ± s.e.m. * =$p<0.05$, ***=$p< 0.001$.

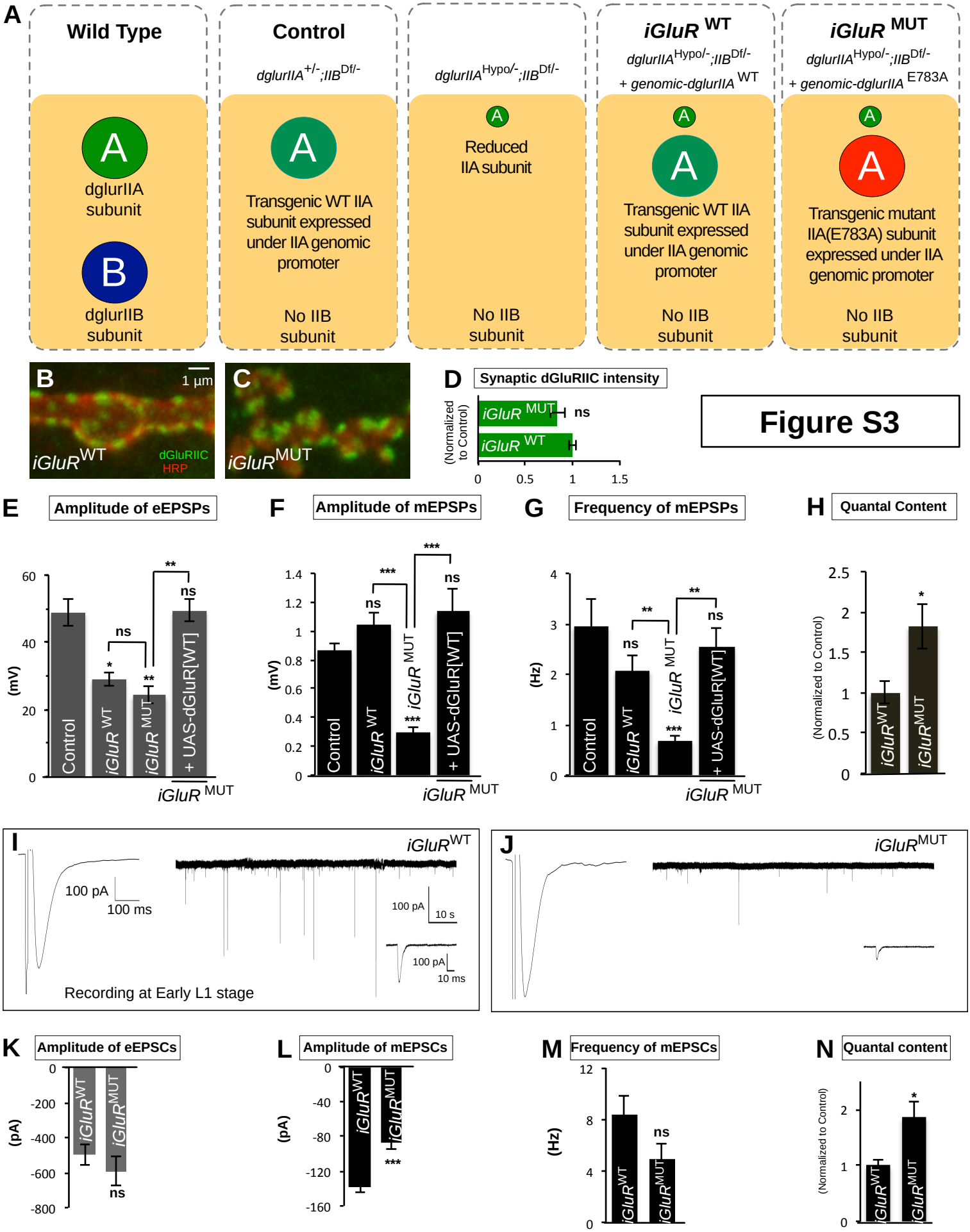
A
Wild Type
dglurIIA subunit
B
dglurIIB subunit
Control
dglurIIA+/-;IIBDf/-
A
Transgenic WT IIA subunit expressed under IIA genomic promoter
No IIB subunit
dglurIIAHypo/-;IIBDf/-
A
Reduced IIA subunit
No IIB subunit
iGluR WT
dglurIIAHypo/-;IIBDf/-
+ genomic-dglurIIA WT
A
A
Transgenic WT IIA subunit expressed under IIA genomic promoter
No IIB subunit
iGluR MUT
dglurIIAHypo/-;IIBDf/-
+ genomic-dglurIIA E783A
A
A
Transgenic mutant IIA(E783A) subunit expressed under IIA genomic promoter
No IIB subunit
B
1 µm
iGluRWT
dGluRIIC
HRP
C
iGluRMUT
D
Synaptic dGluRIIC intensity
(Normalized to Control)
iGluR MUT
ns
iGluR WT
0
0.5
1
1.5
Figure S3
E
Amplitude of eEPSPs
(mV)
60
40
20
0
Control
iGluR WT
iGluR MUT
+ UAS-dGluR[WT]
iGluR MUT
*
**
ns
**
ns
F
Amplitude of mEPSPs
(mV)
1.4
1.2
1
0.8
0.6
0.4
0.2
0
Control
iGluR WT
iGluR MUT
+ UAS-dGluR[WT]
iGluR MUT
***
ns
***
***
ns
G
Frequency of mEPSPs
(Hz)
4
3
2
1
0
Control
iGluR WT
iGluR MUT
+ UAS-dGluR[WT]
iGluR MUT
**
ns
**
***
ns
H
Quantal Content
(Normalized to Control)
2.5
2
1.5
1
0.5
0
iGluRWT
iGluRMUT
*
I
iGluRWT
100 pA
100 ms
100 pA
10 s
100 pA
10 ms
Recording at Early L1 stage
J
iGluRMUT
K
Amplitude of eEPSCs
(pA)
0
-200
-400
-600
-800
iGluRWT
iGluRMUT
ns
L
Amplitude of mEPSCs
(pA)
0
-40
-80
-120
-160
iGluRWT
iGluRMUT
***
M
Frequency of mEPSCs
(Hz)
12
8
4
0
iGluRWT
iGluRMUT
ns
N
Quantal content
(Normalized to Control)
2
1
0
iGluRWT
iGluRMUT
*

Figure S3. iGluR mutant genotypes, abbreviations, synaptic receptor levels, quantification of electrophysiology, Related to Figure 2.

A, Schematic of abbreviations, genotype, subunit composition and description of iGluR mutants in Figure 2. **B,C**, Representative terminals from (B) *iGluR*^{WT} and (C) *iGluR*^{MUT}, labeled with the iGluR subunit, dGluRIIC (green) and the neuronal membrane marker HRP (red). dGluRIIC is an obligatory co-subunit required for functional channels with dGluRIIA. iGluR synaptic clustering is similar in *iGluR*^{WT} and *iGluR*^{MUT}. **D**, Quantification of the ratio of synaptic dGluRIIC intensity to HRP normalized to control ($n \geq 10$). **E-H**, Quantification of (E) the amplitude of eEPSPs, (F) the amplitude of mEPSPs, (G) the frequency of mEPSPs and (H) normalized quantal content (eEPSP amplitude / mEPSP amplitude after correction for nonlinear summation errors) to control ($n \geq 8$) of the indicated genotypes. **I,J**, Representative traces of excitatory post-synaptic current (eEPSC) (left) and miniature excitatory post-synaptic currents (mEPSCs) (right) recorded from early first instar larvae from *iGluR*^{WT} and *iGluR*^{MUT}. **K-N**, Quantification of (K) the amplitude of eEPSCs, (L) the amplitude of mEPSCs, (M) the frequency of mEPSCs and (N) normalized quantal contents (eEPSC amplitude / mEPSC amplitude) to control ($n \geq 5$) of *iGluR*^{WT} and *iGluR*^{MUT}. Scale is the same between images B,C and between I,J. All error bars indicate ± s.e.m. * =$p<0.05$, ***<0.001.

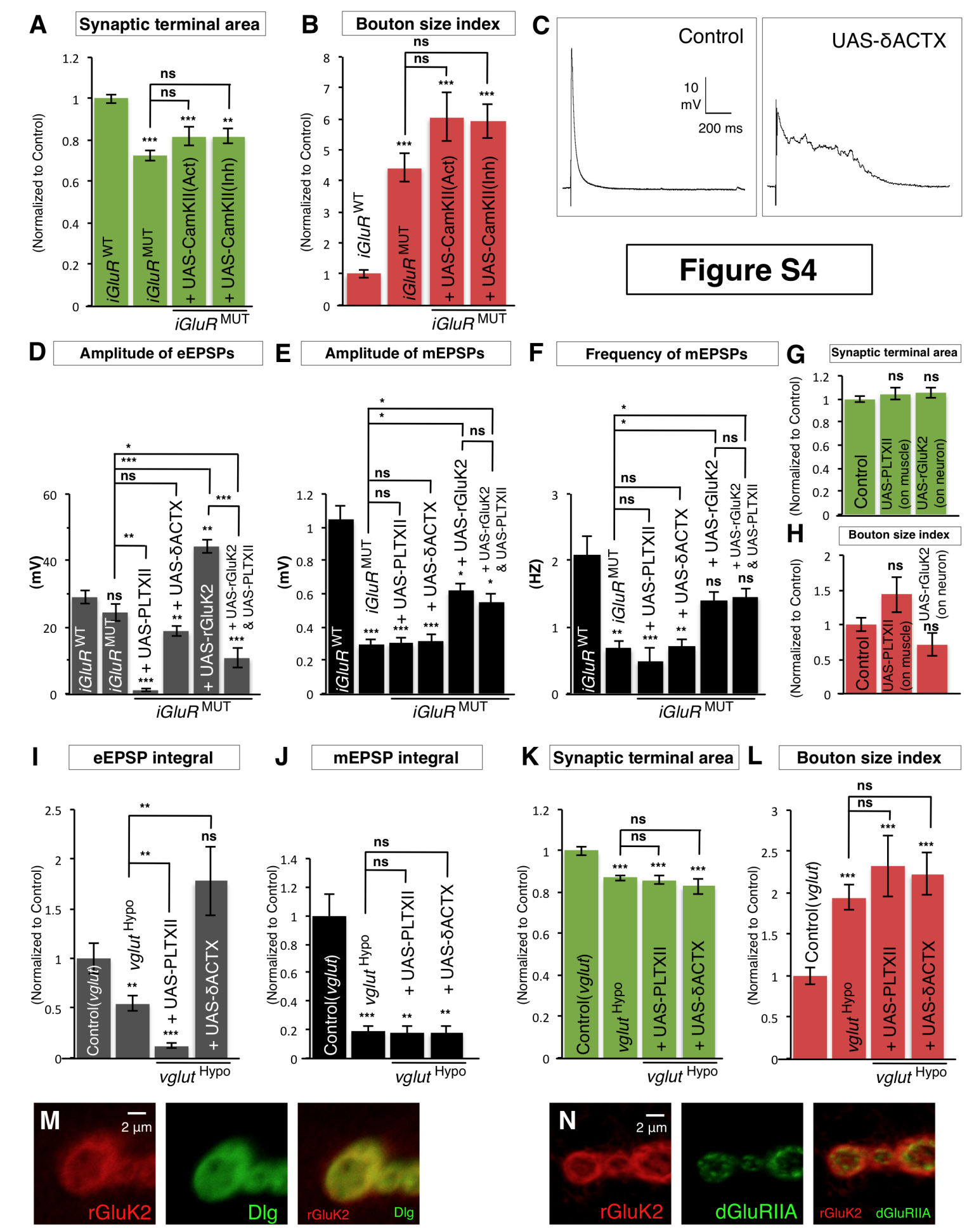
A
Synaptic terminal area
(Normalized to Control)
iGluR WT
iGluR MUT
+ UAS-CamKII(Act)
+ UAS-CamKII(Inh)
iGluR MUT
B
Bouton size index
C
Control
UAS-δACTX
10 mV
200 ms
Figure S4
D
Amplitude of eEPSPs
(mV)
+ UAS-PLTXII
+ UAS-δACTX
+ UAS-rGluK2
+ UAS-rGluK2 & UAS-PLTXII
E
Amplitude of mEPSPs
F
Frequency of mEPSPs
(HZ)
G
Synaptic terminal area
Control
UAS-PLTXII (on muscle)
UAS-rGluK2 (on neuron)
H
Bouton size index
I
eEPSP integral
Control(vglut)
vglut Hypo
vglut Hypo
J
mEPSP integral
K
Synaptic terminal area
L
Bouton size index
M
2 µm
rGluK2
Dlg
rGluK2 Dlg
N
2 µm
rGluK2
dGluRIIA
rGluK2 dGluRIIA

Figure S4. Electrophysiological and morphological quantification and synaptic receptor localization, Related to Figure 2 and Figure 3.

A,B,D-L, Quantification of the NMJ (A,G,K) synaptic terminal area, (B,H,L) bouton size index ($n \geq 17$ for A,B, $n \geq 15$ for G,H and $n \geq 25$ for K,L), (D) the amplitude of eEPSPs, (E) the amplitude of mEPSPs ,(F) the frequency of mEPSPs ($n \geq 8$), (I) eEPSP integral and (J) mEPSP integral ($n \geq 5$) of the indicated genotypes normalized to controls [*iGluR*^{WT} for A,B,D-F, *vglut*$^{Df/+}$ for I-L and CS for G,H]. Detailed description of used genotypes are as follows, ***iGluR*^{MUT}+UAS-CamKII^{Act}** [*dglurIIA*$^{Hypo/-}$*,IIB*$^{Df/-}$*,G14-Gal4;UAS-CamKII*^{T287D}*/genomic-dglurIIA*^{E783A}], ***iGluR*^{MUT}+UAS-CamKII^{Inh}** [*dglurIIA*$^{Hypo/-}$*,IIB*$^{Df/-}$*,G14-Gal4;UAS-CamKIINtide/genomic-dglurIIA*^{E783A}], **Control(*vglut*)** [*vglut*$^{Df/+}$], ***vglut*^{Hypo}**[*vglut*$^{Hypo/Df}$], ***vglut*^{Hypo} + UAS-PLTXII** [*vglut*$^{Hypo/Df}$,*OK319-Gal4;+/UAS-PLTXII*], ***vglut*^{Hypo} + UAS-δACTX** [*vglut*$^{Hypo/Df}$,*OK319-Gal4;+/UAS-δACTX*], **Control** [CS], **UAS-PLTXII (on muscle)** [*G14-Gal4/+;+/UAS-PLTXII*] and **UAS-rGluK2 (on neuron)** [*OK319-Gal4/+;+/UAS-rGluK2*]. **C,** Representative trace of **Control** [CS] and **UAS-δACTX** [*OK319-Gal4/+;+/UAS-δACTX*] **M,N**, Representative terminals from UAS-rGluK2 [*UAS-rGluK2/C57-Gal4*], labled with the rGluK2 (red), Dlg (green for M) or dGluRIIA (green for N). Error bars indicate ± s.e.m. *=$p<0.05$, **= $p<0.01$, ***=$p< 0.001$.

Figure S5

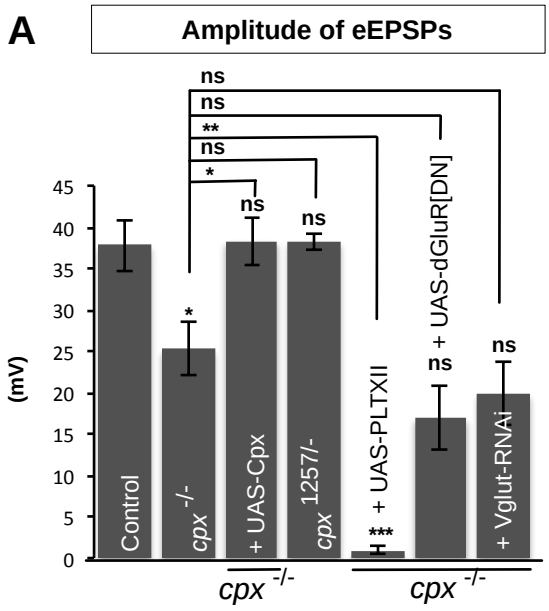
A
Amplitude of eEPSPs
(mV)
Control
cpx -/-
+ UAS-Cpx
1257/- cpx
+ UAS-PLTXII
+ UAS-dGluR[DN]
+ Vglut-RNAi
cpx -/-
cpx -/-

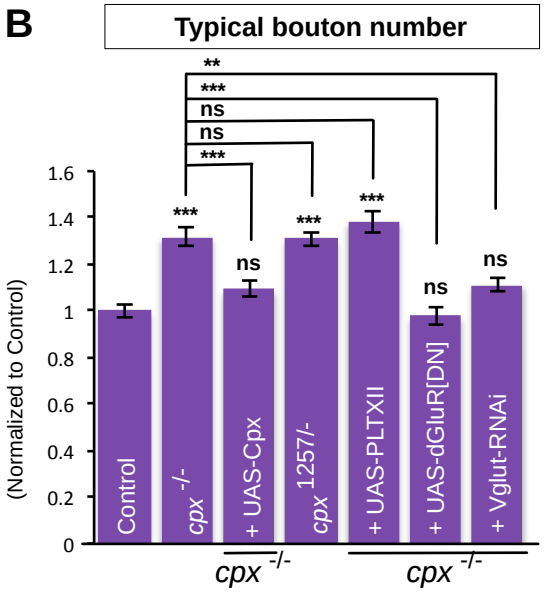
B
Typical bouton number
(Normalized to Control)
Control
cpx -/-
+ UAS-Cpx
1257/- cpx
+ UAS-PLTXII
+ UAS-dGluR[DN]
+ Vglut-RNAi
cpx -/-
cpx -/-

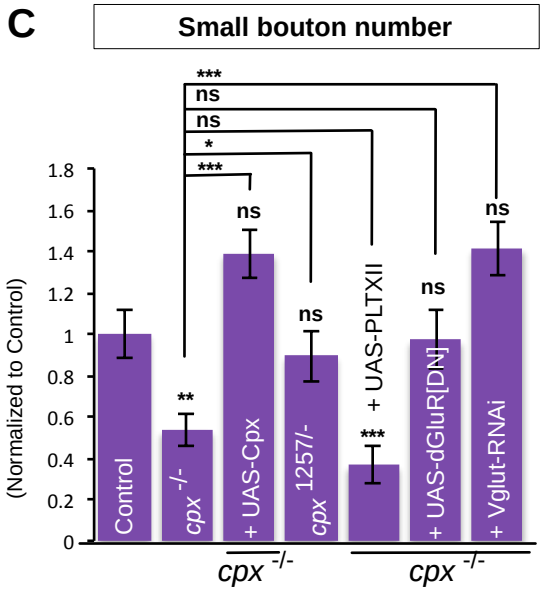
C
Small bouton number
(Normalized to Control)
Control
cpx -/-
+ UAS-Cpx
1257/- cpx
+ UAS-PLTXII
+ UAS-dGluR[DN]
+ Vglut-RNAi
cpx -/-
cpx -/-

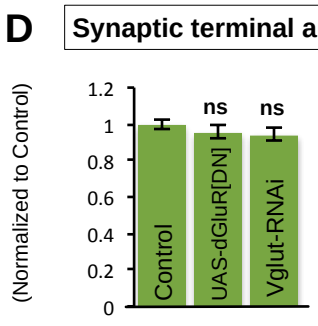
D
Synaptic terminal area
(Normalized to Control)
Control
UAS-dGluR[DN]
Vglut-RNAi

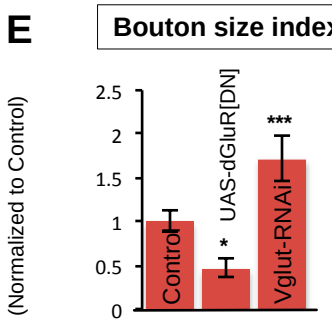
E
Bouton size index
(Normalized to Control)
Control
UAS-dGluR[DN]
Vglut-RNAi

Figure S5. Electrophysiological and morphological quantification of *cpx* mutants, Related to Figure 4.

A-D, Quantification of NMJ (A) the amplitude of eEPSPs (n≥8), (B) typical bouton number, (C) small bouton number (n≥35), (D) synaptic terminal area and (E) bouton size index (n≥28) of the indicated genotypes normalized to controls [*cpx* $^{Df/+}$ for B,C and CS for D,E]. Detailed description of used genotypes are followed, **UAS-dGluR^{DN}** [*G14-Gal4/+;+/UAS-dglurIIA*^{E783A}] and **Vglut-RNAi** [*OK6-Gal4/UAS-Vglut-RNAi*^{KK}]. All error bars indicate ± s.e.m. * =p<0.05, **= p<0.01, ***=p< 0.001.

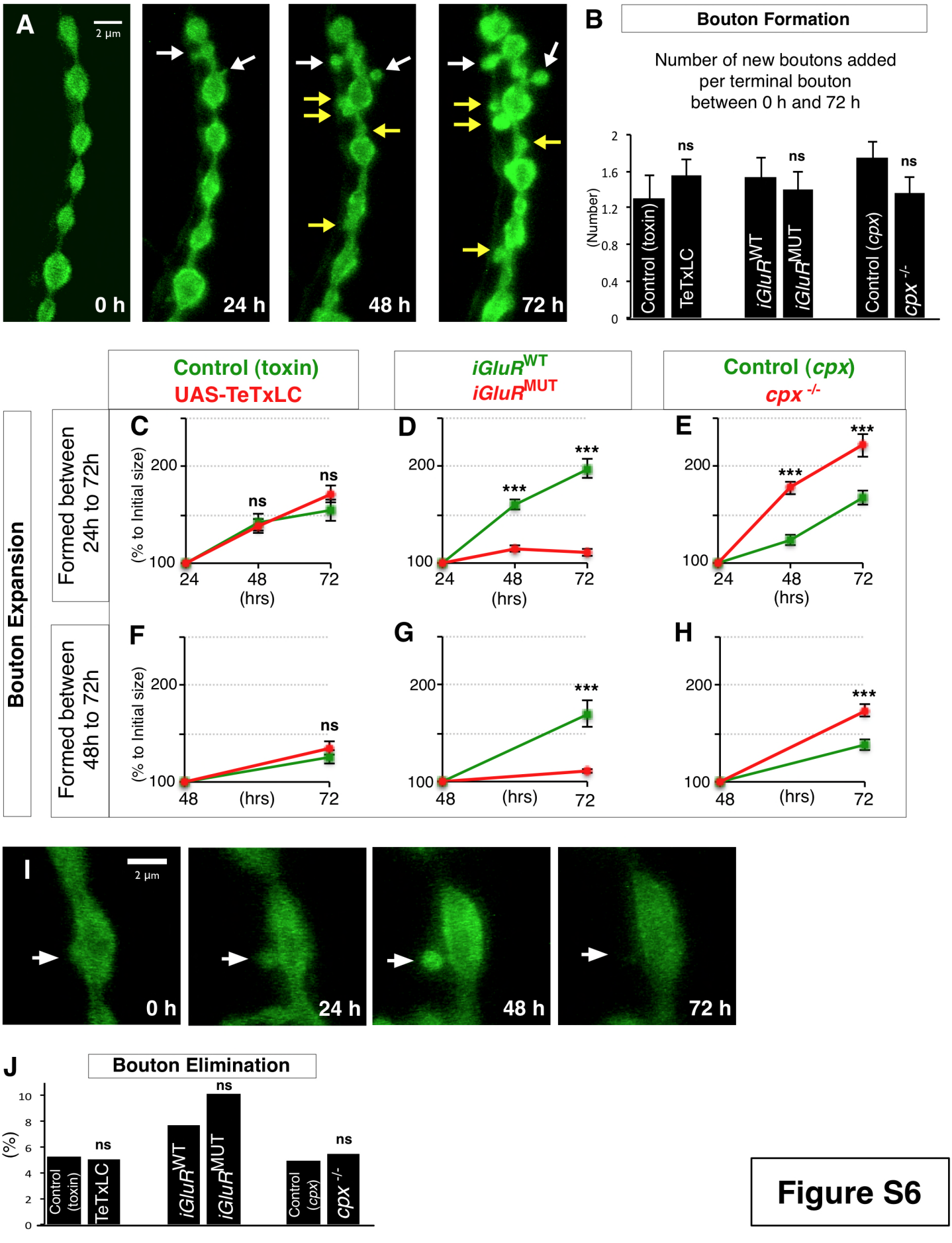
A
2 µm
0 h
24 h
48 h
72 h
B
Bouton Formation
Number of new boutons added per terminal bouton between 0 h and 72 h
(Number)
Control (toxin)
TeTxLC
iGluR^WT
iGluR^MUT
Control (cpx)
cpx -/-
ns
Control (toxin) UAS-TeTxLC
iGluR^WT iGluR^MUT
Control (cpx) cpx -/-
Bouton Expansion
Formed between 24h to 72h
Formed between 48h to 72h
(% to Initial size)
(hrs)
C
D
E
F
G
H
***
I
J
Bouton Elimination
(%)

Figure S6

Figure S6. Time-lapse images and measurement of bouton formation, expansion and elimination, Related to Figure 5.

A, Representative time-lapse images of synaptic boutons from control [*Vglut-lexA,LexOp-CD8-GFP*/+] at muscles 1/9 labeled with membrane tagged GFP expressed in all MNs. Arrows indicate new immature boutons formed between 0h-24h (white) or 24h-48h (yellow). **B**, Quantification of the number of new boutons added from terminal boutons (n≥26 terminal boutons from n≥7 NMJs) for indicated genotypes. **C-H**, Quantification of the bouton size expansion during time-lapse imaging period (n≥41 boutons from n≥7 NMJs for C-E, n≥18 boutons from n≥7 NMJs for F-H) for indicated genotypes. Imaging period is from 24h to 72h for C-E and from 48h to 72h for F-H. All data are normalized to initial bouton size. **I**, Representative time-lapse synaptic boutons of control [*Vglut-lexA,LexOp-CD8-GFP*/+] at muscle 1/9 labeled with membrane tagged GFP expressed at all MNs. Arrows indicate an eliminated bouton. **J,** Quantification of the percentage of bouton elimination for indicated genotypes (n≥113 of all boutons from n≥7 NMJs). Elimination was scored as the disappearance of bouton between imaging periods. These events are likely not analogous to synaptic 'retractions' as among 113 boutons imaged in control animals we confirmed only a single synaptic 'foot-print' (Dlg staining without presynaptic HRP marker). Scale is the same for images in A and I. For (J), p value was calculated by Fisher's exact test between mutant and control. All error bars indicate ± s.e.m. * =p<0.05, ***=p< 0.001.

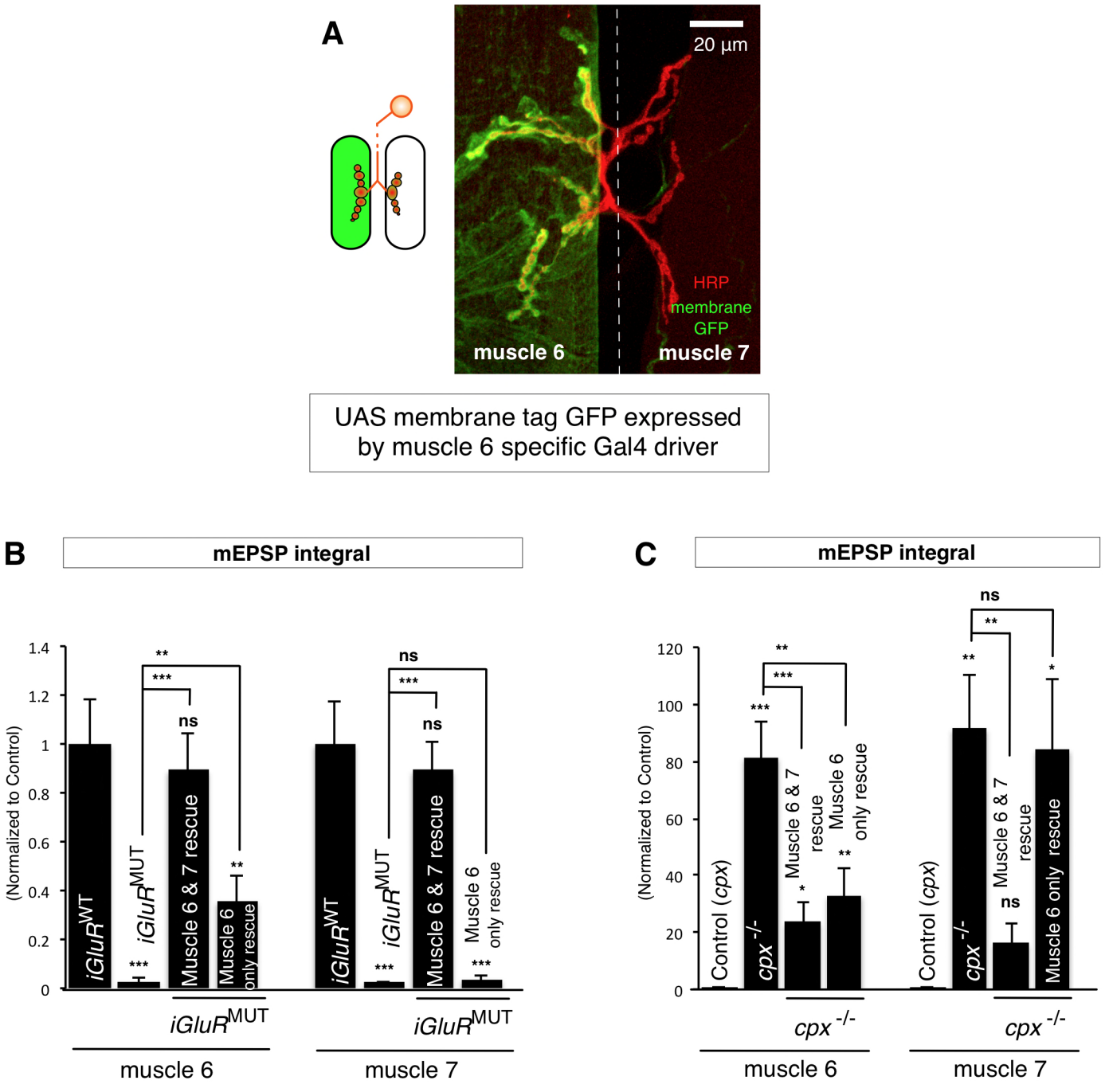
A
20 µm
HRP
membrane
GFP
muscle 6
muscle 7
UAS membrane tag GFP expressed
by muscle 6 specific Gal4 driver
B
mEPSP integral
(Normalized to Control)
iGluR^WT
iGluR^MUT
Muscle 6 & 7 rescue
Muscle 6 only rescue
iGluR^MUT
muscle 6
muscle 7
C
mEPSP integral
(Normalized to Control)
Control (cpx)
cpx -/-
Muscle 6 & 7 rescue
Muscle 6 only rescue
cpx -/-
muscle 6
muscle 7

Figure S7

Figure S7. Representative Muscle 6 specific Gal4 image and electrophysiological quantification, Related to Figure 7.

A, Representative RP3 terminals at muscle 6 and muscle 7, segment A3 from late third instar larvae stage animals labeled with membrane tagged GFP (Green) and neuronal membrane marker HRP (red). UAS-CD8-GFP was expressed with the muscle 6 specific Gal4 driver combination H94-Gal4,nSyb-Gal80 combined with tub^{P}>stop>Gal4, UAS-FLP. The tub^{P}>stop>Gal4 construct was used to demonstrate that the H94-Gal4,nSyb-Gal80 combination does not produce Gal4 in muscle 7 throughout experimental period. **B,C**, Quantification of the mEPSP integral for indicated genotypes ($n \geq 8$ for B, $n \geq 5$ for C).

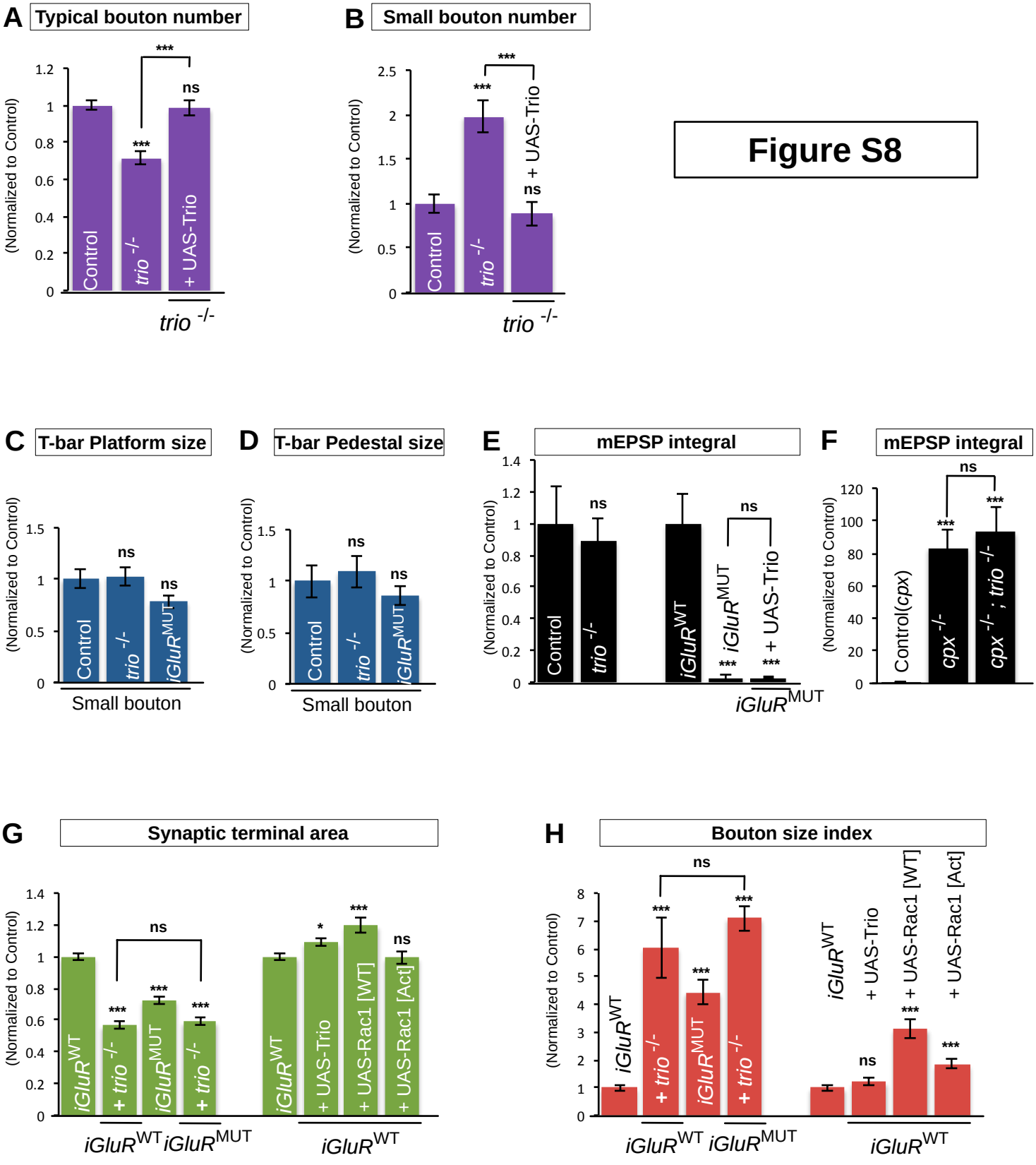
A
Typical bouton number
(Normalized to Control)
Control
trio -/-
+ UAS-Trio
trio -/-
B
Small bouton number
(Normalized to Control)
Control
trio -/-
+ UAS-Trio
trio -/-
Figure S8
C
T-bar Platform size
(Normalized to Control)
Control
trio -/-
iGluRMUT
Small bouton
D
T-bar Pedestal size
(Normalized to Control)
Control
trio -/-
iGluRMUT
Small bouton
E
mEPSP integral
(Normalized to Control)
Control
trio -/-
iGluRWT
iGluRMUT
+ UAS-Trio
iGluRMUT
F
mEPSP integral
(Normalized to Control)
Control(cpx)
cpx -/-
cpx -/- ; trio -/-
G
Synaptic terminal area
(Normalized to Control)
iGluRWT
+ trio -/-
iGluRMUT
+ trio -/-
iGluRWT
+ UAS-Trio
+ UAS-Rac1 [WT]
+ UAS-Rac1 [Act]
iGluRWT iGluRMUT
iGluRWT
H
Bouton size index
(Normalized to Control)
iGluRWT
+ trio -/-
iGluRMUT
+ trio -/-
iGluRWT
+ UAS-Trio
+ UAS-Rac1 [WT]
+ UAS-Rac1 [Act]
iGluRWT iGluRMUT
iGluRWT

Figure S8. Electrophysiological and morphological quantification, Related to Figure 8.

A,B,G,H, Quantification of NMJs including (A) typical bouton number, (B) small bouton number, (G) synaptic terminal area and (H) the bouton size index for indicated genotypes (n≥23 for A,B and n≥22 for G,H). **C,D**, Quantification of the size of T-bar of small bouton from control [CS], *trio* $^{-/-}$ mutant and *iGluR* ^{MUT} mutant (n≥10). **E,F,** Quantification of the mEPSP integral for indicated genotypes (n≥10 for E and n≥8 for F). Control is [CS] (for A-E) and [*cpx*$^{Df/+}$] (for F). All quantification data are normalized to control. Detailed description of used genetypes are followed, Control [CS], Control(*cpx*) [*cpx*$^{Df/+}$], ***trio*$^{-/-}$** mutant [*trio*$^{-/-}$], ***trio*$^{-/-}$ + UAS-Trio** [*UAS-Trio/+;+/OK319-Gal4;trio*$^{-/-}$], ***iGluR*^{WT}** [*dglurIIA*$^{Hypo/-}$*,IIB*$^{Df/-}$*;+/genomic-dglurIIA*^{WT}], ***iGluR*^{MUT}** [*dglurIIA*$^{Hypo/-}$*,IIB*$^{Df/-}$*;+/genomic-dglurIIA*^{E783A}], ***iGluR*^{WT} + *trio*$^{-/-}$** [*dglurIIA*$^{Hypo/-}$*,IIB*$^{Df/-}$*; trio*$^{-/-}$*,genomic-dglurIIA*^{WT}], ***iGluR*^{MUT} + *trio*$^{-/-}$**[*dglurIIA*$^{Hypo/-}$*,IIB*$^{Df/-}$*; trio*$^{-/-}$*,genomic-dglurIIA*^{E783A}], ***iGluR*^{WT} + UAS-Trio** [*dglurIIA*$^{Hypo/-}$*,IIB*$^{Df/-}$*,OK319-Gal4;UAS-Trio/genomic-dglurIIA*^{WT}], ***iGluR*^{WT} + UAS-Rac1^{WT}** [*dglurIIA*$^{Hypo/-}$*,IIB*$^{Df/-}$*,OK319-Gal4;UAS-Rac1*^{WT}*/genomic-dglurIIA*^{WT}] and ***iGluR*^{WT} + UAS-Rac1^{Act}** [*dglurIIA*$^{Hypo/-}$*,IIB*$^{Df/-}$*,OK319-Gal4;UAS-Rac1*^{V12}*/genomic-dglurIIA*^{WT}]. All error bars indicate ± s.e.m. * =p<0.05, **= p<0.01, ***=p< 0.001.

Supplemental Methods

Genetics

The following Gal4 stocks were used: ***OK319-Gal4*** (Beck et al., 2012). OK319-Gal4 is expressed only in the ISN subset of motor neurons (MNs) that includes the motor neurons innervating muscle 4 (morphological analysis), muscles 6 & 7 (morphological & electrophysiological analysis) and muscles 1 & 9 (time-lapse live imaging) beginning in late embryos and continuing throughout larval development until pupation, ***OK6-Gal4*** - Expressed in all larval MNs from late embryos to pupation (Aberle et al., 2002), ***D42-Gal4*** - Expressed in all larval MNs (Yeh et al., 1995), ***G14-Gal4*** - Expressed in larval muscles including muscle 4, 6 and 7 (Aberle et al., 2002), ***C57-Gal4*** - Expressed in larval muscles including muscle 4, 6 and 7 (Budnik et al., 1996), ***H94-Gal4,nSyb-Gal80*** – Expressed in subset of larval muscles including muscles 6 but not muscle 7 (Davis and Goodman, 1998; Rubinstein et al., 2010). Specificity throughout development was confirmed by crossing with *tub^{P}>stop>Gal4, UAS-FLP, UAS-CD8-GFP* (Figure S7A) (Roy et al., 2007).

The following existing transgenic stocks were used: **UAS-TeTxLC** [TNTE] (Sweeney et al., 1995), **UAS-Vglut-RNAi** (UAS-Vglut-RNAi^{JF}, JF02689, target 1278-1724nt of *vglut* transcript) (Figure 1,S1), (UAS-Vglut-RNAi^{HMS}, HMS02011, target 3077-3098nt), (Ni et al., 2008) (Figure S1) or (UAS-Vglut-RNAi^{KK}, VDRC104324, target 1279-1900nt) (Dietzl et al., 2007), (Figure 1,4,S1,S5), **UAS-Vglut** (Daniels et al., 2004), **genomic-*dglurIIA*^{WT}** (DiAntonio et al., 1999), **genomic-*dglurIIA*Δ3UTR** (Schmid et al., 2006), **genomic-*dglurIIA*^{E783A}** (Schmid et al., 2006), **UAS-CamKII^{Act}** (UAS-CamKII^{T287D}) (Haghighi et al., 2003), **UAS-CamKII^{Inh}** (UAS-CamKIINtide) (Haghighi et al., 2003), **UAS-Cpx** (Huntwork and Littleton, 2007), **Vglut-LexA** (Baek et al.,

2013), **LexOp-CD8-GFP** (Baek et al., 2013), **UAS-Trio** (Bateman et al., 2000), **UAS-Rac1^{WT}** (Luo et al., 1994), **UAS-Rac1^{Act}** (UAS-Rac1^{V12}) (Luo et al., 1994).

The following mutant allele stocks were used: ***dglurIIA^{-},B^{-}*** *(dglurIIA,B^{sp22} = dglurIIA and dglurIIB* double null mutant)(DiAntonio et al., 1999), ***dglurIIA^{Df},B^{Df}*** (*Df(2L)cl^{h4}* = deficiency covering both *dglurIIA and dglurIIB*) (DiAntonio et al., 1999)**,** ***dglurIIA^{Hypo},B^{Df}*** (*Df(2L)cl^{h4}*,genomic-*dglurIIA*Δ3UTR), ***vglut^{Hypo}*** (***vglut^{1}*** = *vglut* hypomorphic allele) (Daniels et al., 2006), ***vglut^{Df}*** (*vglut^{OK371ΔD}* = small deficiency covering *vglut*) (Mahr and Aberle, 2006), ***cpx^{-}*** (*cpx^{SH1}* = *cpx* null allele) (Huntwork and Littleton, 2007), ***cpx^{1257}*** (Iyer et al., 2013), ***cpx^{Df}*** (*Df(3R)ED5021* = deficiency covering *cpx*) (Huntwork and Littleton, 2007), ***trio^{-}*** (*trio^{S137203}* = *trio* null allele) (Bateman et al., 2000).

The following allelic combinations were used (DiAntonio et al., 1999; Schmid et al., 2006; Steinert et al., 2006): **CS**: CantonS, ***dgluRIIA$^{+/-}$,IIB$^{-/Df}$*** (Control in Figure 2)**:** *dglurIIA,B^{sp22}/Df(2L)cl^{h4}*;+/genomic-*dglurIIA^{WT}*, ***dgluRIIA$^{Hypo/-}$,IIB$^{-/Df}$:*** *dglurIIA,B^{sp22}/Df(2L)cl^{h4}*,genomic-*dglurIIA*Δ3UTR, ***iGluR^{WT}:*** *dglurIIA,B^{sp22}/Df(2L)cl^{h4}*,genomic-*dglurIIA*Δ3UTR;+/genomic-*dglurIIA^{WT}*, ***iGluR^{MUT}***: *dglurIIA,B^{sp22}/Df(2L)cl^{h4}*,genomic-*dglurIIA*Δ3UTR;+/genomic-*dglurIIA^{E783A}*, **Control (*vglut*) or *vglut$^{Df/+}$***: *vglut^{OK371ΔD}*/+, ***vglut^{MN}***: *vglut^{1}*,*UAS-Vglut-vRNAi^{VDRC104324}*/ *vglut^{OK371ΔD}*;*D42-Gal4*/*UAS-Vglut-RNAi^{JF02689}*, **Vglut-RNAi#1**: *UAS-Vglut-RNAi^{VDRC104324}/+;UAS-Vglut-RNAi^{JF02689}/D42-Gal4*, **Vglut-RNAi#2**: *OK6-Gal4/+;D42-Gal4/UAS-Vglut-RNAi^{HMS},* ***vglut$^{Hypo/Df}$*** : *vglut^{1}/vglut^{OK371ΔD}* **,Control (*cpx*) or *cpx$^{Df/+}$***: *Df(3R)ED5021*/+, ***cpx$^{-/-}$:*** *Df(3R)ED5021*/*cpx^{SH1}*, ***cpx$^{1257/-}$:*** *Df(3R)ED5021*/*cpx^{1257}* , , ***trio$^{-/-}$:*** *trio^{S137203}*/ *trio^{S137203}*. Controls used for each genotype are in figure legends and/or Table S1.

Molecular Biology.

The following transgenes were constructed:

UAS-dGluR^{WT} – Full length *dglurIIA* cDNA.

UAS-dGluR^{DN} –*dglurIIA* cDNA with Glutamic acid at position 783 to mutated to Alanine. This mutation results in a receptor that is correctly localized but non-functional (Schmid et al., 2006).

UAS-rGluK2 – Full length rat GluK2 cDNA (gift from Dr. R.E. Oswald, Cornell University, Ithaca, NY).

UAS-PLTXII and **UAS-δACTX**. – These membrane-tethered toxins are expressed as chimeric fusion proteins comprising (from N to C termini), the secretory signal sequence from Lynx1, native mammalian prototoxin, mature cleaved peptide toxin sequence, glycine-asparagine repeat hydrophilic linker and the Lynx1 GPI targeting sequence (Wu et al., 2008). The complete amino sequence for both toxin peptides are

PLTXII:

MSALLILALVGAAVAADCSATGDTCDHTKKCCDDCYTCRCGTPWGANCRCDYYKARCDTGNG
NGNGNGEQKLISEEDlgNGNGNGNGNGNGNGDGNGGALCNGAGFATPVTLALVPALLATFWS
LL*

δACTX:

MSALLILALVGAAVACAKKRNWCGKTEDCCCPMKCVYAWYNEQGSCQSTISALWKKCGNGN
GNGNGEQKLISEEDlgNGNGNGNGNGNGNGDGNGGALCNGAGFATPVTLALVPALLATFWSLL
*

dGluR^{WT}, dGluR^{DN} and rGluK2 were cloned into pBID-UAS-G and transgenes generated using Phi3C1 site-directed transgenesis (Wang et al., 2012). PLTXII and δACTX were cloned into pUAST (Brand and Perrimon, 1993) and transgenes generated using conventional P-element transgenesis.

Electrophysiology

Intracellular recordings from muscle 6, segment A3 or A4 were performed as previously described (Imlach and McCabe, 2009; McCabe et al., 2003) except for Figure S7 where muscle 6 or 7, segment A3 was used. Briefly, third instar larvae were dissected (0.1mM Ca^{2+}) and recordings carried out in HL3 saline containing 1.5mM Ca^{2+} (physiologically relevant Ca^{2+} concentration). Data was only analyzed from recordings where the resting membrane potential was less than –55 mV. Recordings were performed using an Axoclamp 2B amplifier. Data were low-pass filtered at 1 kHz, digitized, and recorded to disk using a Digidata 1322A interface. eEPSPs, mEPSPs amplitudes, frequency and integrals were measured using the peak detection feature of MiniAnalysis program (Synaptosoft, Inc.). For early first instar larvae recordings, larvae were dissected (0.1mM Ca^{2+}) and recorded in HL3 saline containing 1.0 mM Ca^{2+}. Muscle 6 was whole-cell voltage clamped and mini EPSCs were recorded for 2 min at a holding potential of -80mV. eEPSCs were evoked by stimulating the appropriate segmental nerve with a pulse of 5-8 V that lasted 1ms using a suction electrode. Recordings were made using a Multiclamp 700B amplifier controlled by pClamp 10.2 (Molecular Devices, Sunnyvale, CA). Sampling frequency was 20kHz and traces were filtered at 10kHZ. Data was analysed in Clampfit 10.2, mEPSCs were detected semi-automatic and amplitudes were measured using the event detection tool. **Quantal content** was calculated for each individual recording by calculating (eEPSP amplitude / mEPSP amplitude) (Frank et al., 2006) after correction for nonlinear summation errors (Martin, 1955).

Immunohistochemistry

Wandering third instar larva of comparable size were collected, dissected, and stained as previously described (Brent et al., 2009a; Brent et al., 2009b; McCabe et al., 2003). Briefly,

animals were dissected in 1x PBS (Mediatech) and fixed for 20 minutes in 4% formaldehyde (Sigma-Aldrich). Animals were washed multiple times in PBT (PBS + 0.1% Triton) and then blocked in PBTB (PBT + 0.2% BSA) and PBTN (PBTB+ 2% Normal Goat Serum). Primary antibodies used were mouse anti-Dlg (1:500; Developmental Studies Hybridoma Bank (DSHB) at the University of Iowa), mouse anti-Brp (Wagh et al., 2006) (Nc82, 1:100; DSHB), mouse anti-FasII (1D4, 1:500; DSHB), rabbit anti-Syt1 (1:1000, gift from Troy Littleton, M.I.T., Cambridge, MA), rabbit anti-GluR6/GluK2 (1:1000, Millipore) and rabbit anti-DGluRIII/IIC (Marrus et al., 2004) (1:500, gift from Aaron DiAntonio, Washington University, Saint Louis, MO). Animals were incubated overnight at 4^{o}C in primary antibodies, washed in PBTB and PBTN, and then incubated in secondary antibodies for 2 hours at room temperature. Secondary antibodies used included goat anti-mouse Alexa-488 (1:1000; Invitrogen), goat anti-rabbit Alexa-555 (1:1000; Invitrogen), goat aniti-mouse Cy3 (1:1000; Jackson ImmunoResearch) and Cy5 conjugated HRP (1:400; Jackson ImmunoResearch). Imaging was carried out on Zeiss 510 confocal microscope. To compare intensity levels, experimental and control animals were stained in the same tube and imaged using identical confocal settings and then a maximum projection rendering of z-stacks was analyzed for signal intensity using MetaMorph software (Molecular Devices, Downingtown, PA). Synaptic area was identified by HRP. Intensity was normalized against HRP. For Figure S1D, **the relative frequency histogram of the distribution of bouton sizes**, boundaries of individual boutons were identified manually while blinded to genotype, by using round regional tool of MetaMorph software.

Time-lapse live imaging

Presynaptic motor neurons were labeled with membrane localized LexOp-CD8-GFP expressed by vglut-LexA in both control and mutant backgrounds. All glutamatergic neurons including all type I motor neurons were labeled. Animals were anesthetized by ~15 minute exposure to a

vapor mixture of 35% Methyl Salicylate and 16% Menthol (Haw Par Healthcare Ltd., Singapore) every 24 hours from the second instar onwards for 4 days. For imaging, larva were placed on a slide with 70% glycerol and cover slip. Imaging time was limited to less than 30 minutes after which animals were washed gently with PBS, allowed to recover and returned to the food media. Mutants and corresponding controls were imaged on the same day in a random order to minimize handling variability. For each time point, confocal images (63x, oil immersion lens) of an NMJ terminal z-stack were captured. Type Ib NMJ terminal on muscle 1 or 9 of segment A3 to A6 were chosen for imaging due to exterior localization of these NMJs in muscle field and labeling by the OK319-Gal4 driver. After time-lapse imaging was complete, each animal was dissected, fixed and stained by HRP and Dlg to confirm bouton type. Only images from animals that survived the entire 4-day imaging procedure were included in analysis. For **bouton size expansion in live images**, the size of each bouton was measured using the round regional tool of MetaMorph software while blinded to genotype. Only initial sizes smaller than $2\mu m^2$ (categorized as small bouton) were subjected for analysis throughout imaging period. For **the bouton formation in live images**, only most distal bouton was used for analysis which can be reliably recognized in live imaging. The number of new boutons added between 0h to 72h were counted. For **bouton elimination**, the number of boutons that were lost during 24h to 72h were counted. No bouton re-appeared once eliminated during the imaging period.

Electron microscopy

Fillets from third instar larvae were dissected in HL3 without Ca^{2+} (Jiao et al., 2010a; Jiao et al., 2010b; McCabe et al., 2003). Fillets were then incubated in HL3 buffer containing EDTA for 10 min for resting conditions. The specimens were fixed in 3% glutaraldehyde and 0.5% paraformaldehyde in PBS (pH 7.2) overnight in cold room. Fillets were washed with PBS and postfixed in 1% OsO4, dehydrated in alcohol, and embedded in Durcupan ACM (Fluka). Serial

ultrathin sections were cut with a diamond knife (Diatome), collected on grids and stained with 1% uranyl acetate and lead citrate. The grids were then examined with a JEOL 1200 electron microscope. Images were quantified with NIH ImageJ software.

Supplemental References

Aberle, H., Haghighi, A.P., Fetter, R.D., McCabe, B.D., Magalhães, T.R., and Goodman, C.S. (2002). wishful thinking encodes a BMP type II receptor that regulates synaptic growth in Drosophila. Neuron *33*, 545-558.

Baek, M., Enriquez, J., and Mann, R.S. (2013). Dual role for Hox genes and Hox co-factors in conferring leg motoneuron survival and identity in Drosophila. Development *140*, 2027-2038.

Bateman, J., Shu, H., and Van Vactor, D. (2000). The guanine nucleotide exchange factor trio mediates axonal development in the Drosophila embryo. Neuron *26*, 93-106.

Beck, E.S., Gasque, G., Imlach, W.L., Jiao, W., Jiwon Choi, B., Wu, P.-S., Kraushar, M.L., and McCabe, B.D. (2012). Regulation of Fasciclin II and synaptic terminal development by the splicing factor beag. J Neurosci *32*, 7058-7073.

Brand, A.H., and Perrimon, N. (1993). Targeted gene expression as a means of altering cell fates and generating dominant phenotypes. Development *118*, 401-415.

Brent, J., Werner, K., and McCabe, B.D. (2009a). Drosophila larval NMJ immunohistochemistry. Journal of visualized experiments : JoVE, e1108.

Brent, J.R., Werner, K.M., and McCabe, B.D. (2009b). Drosophila larval NMJ dissection. Journal of visualized experiments : JoVE, e1107.

Budnik, V., Koh, Y.H., Guan, B., Hartmann, B., Hough, C., Woods, D., and Gorczyca, M. (1996). Regulation of synapse structure and function by the Drosophila tumor suppressor gene dlg. Neuron *17*, 627-640.

Daniels, R.W., Collins, C.A., Chen, K., Gelfand, M.V., Featherstone, D.E., and DiAntonio, A. (2006). A single vesicular glutamate transporter is sufficient to fill a synaptic vesicle. Neuron *49*, 11-16.

Daniels, R.W., Collins, C.A., Gelfand, M.V., Dant, J., Brooks, E.S., Krantz, D.E., and DiAntonio, A. (2004). Increased expression of the Drosophila vesicular glutamate transporter leads to excess glutamate release and a compensatory decrease in quantal content. J Neurosci *24*, 10466-10474.

Davis, G.W., and Goodman, C.S. (1998). Synapse-specific control of synaptic efficacy at the terminals of a single neuron. Nature *392*, 82-86.

DiAntonio, A., Petersen, S.A., Heckmann, M., and Goodman, C.S. (1999). Glutamate receptor expression regulates quantal size and quantal content at the Drosophila neuromuscular junction. J Neurosci *19*, 3023-3032.

Dietzl, G., Chen, D., Schnorrer, F., Su, K.-C., Barinova, Y., Fellner, M., Gasser, B., Kinsey, K., Oppel, S., Scheiblauer, S*., et al.* (2007). A genome-wide transgenic RNAi library for conditional gene inactivation in Drosophila. Nature *448*, 151-156.

Frank, C.A., Kennedy, M.J., Goold, C.P., Marek, K.W., and Davis, G.W. (2006). Mechanisms underlying the rapid induction and sustained expression of synaptic homeostasis. Neuron *52*, 663-677.

Haghighi, A.P., McCabe, B.D., Fetter, R.D., Palmer, J.E., Hom, S., and Goodman, C.S. (2003). Retrograde control of synaptic transmission by postsynaptic CaMKII at the Drosophila neuromuscular junction. Neuron *39*, 255-267.

Huntwork, S., and Littleton, J.T. (2007). A complexin fusion clamp regulates spontaneous neurotransmitter release and synaptic growth. Nat Neurosci *10*, 1235-1237.

Imlach, W., and McCabe, B.D. (2009). Electrophysiological methods for recording synaptic potentials from the NMJ of Drosophila larvae. Journal of visualized experiments : JoVE, e1109.

Iyer, J., Wahlmark, C.J., Kuser-Ahnert, G.A., and Kawasaki, F. (2013). Molecular mechanisms of COMPLEXIN fusion clamp function in synaptic exocytosis revealed in a new Drosophila mutant. Mol Cell Neurosci *56C*, 244-254.

Jiao, W., Masich, S., Franzén, O., and Shupliakov, O. (2010a). Two pools of vesicles associated with the presynaptic cytosolic projection in Drosophila neuromuscular junctions. J Struct Biol *172*, 389-394.

Jiao, W., Shupliakov, A., and Shupliakov, O. (2010b). A semi-correlative technique for the subcellular localization of proteins in Drosophila synapses. J Neurosci Methods *185*, 273-279.

Luo, L., Liao, Y.J., Jan, L.Y., and Jan, Y.N. (1994). Distinct morphogenetic functions of similar small GTPases: Drosophila Drac1 is involved in axonal outgrowth and myoblast fusion. Genes Dev *8*, 1787-1802.

Mahr, A., and Aberle, H. (2006). The expression pattern of the Drosophila vesicular glutamate transporter: a marker protein for motoneurons and glutamatergic centers in the brain. Gene Expr Patterns *6*, 299-309.

Marrus, S.B., Portman, S.L., Allen, M.J., Moffat, K.G., and DiAntonio, A. (2004). Differential localization of glutamate receptor subunits at the Drosophila neuromuscular junction. J Neurosci *24*, 1406-1415.

Martin, A.R. (1955). A further study of the statistical composition on the end-plate potential. J Physiol (Lond) *130*, 114-122.

McCabe, B.D., Marqués, G., Haghighi, A.P., Fetter, R.D., Crotty, M.L., Haerry, T.E., Goodman, C.S., and O'Connor, M.B. (2003). The BMP homolog Gbb provides a retrograde signal that regulates synaptic growth at the Drosophila neuromuscular junction. Neuron *39*, 241-254.

Ni, J.-Q., Markstein, M., Binari, R., Pfeiffer, B., Liu, L.-P., Villalta, C., Booker, M., Perkins, L., and Perrimon, N. (2008). Vector and parameters for targeted transgenic RNA interference in Drosophila melanogaster. Nat Methods *5*, 49-51.

Roy, B., Singh, A.P., Shetty, C., Chaudhary, V., North, A., Landgraf, M., Vijayraghavan, K., and Rodrigues, V. (2007). Metamorphosis of an identified serotonergic neuron in the Drosophila olfactory system. Neural Dev *2*, 20.

Rubinstein, C.D., Rivlin, P.K., and Hoy, R.R. (2010). Genetic feminization of the thoracic nervous system disrupts courtship song in male Drosophila melanogaster. J Neurogenet *24*, 234-245.

Schmid, A., Qin, G., Wichmann, C., Kittel, R.J., Mertel, S., Fouquet, W., Schmidt, M., Heckmann, M., and Sigrist, S.J. (2006). Non-NMDA-type glutamate receptors are essential for maturation but not for initial assembly of synapses at Drosophila neuromuscular junctions. J Neurosci *26*, 11267-11277.

Steinert, J.R., Kuromi, H., Hellwig, A., Knirr, M., Wyatt, A.W., Kidokoro, Y., and Schuster, C.M. (2006). Experience-dependent formation and recruitment of large vesicles from reserve pool. Neuron *50*, 723-733.

Sweeney, S.T., Broadie, K., Keane, J., Niemann, H., and O'Kane, C.J. (1995). Targeted expression of tetanus toxin light chain in Drosophila specifically eliminates synaptic transmission and causes behavioral defects. Neuron *14*, 341-351.

Wagh, D.A., Rasse, T.M., Asan, E., Hofbauer, A., Schwenkert, I., Dürrbeck, H., Buchner, S., Dabauvalle, M.-C., Schmidt, M., Qin, G.*, et al.* (2006). Bruchpilot, a protein with homology to ELKS/CAST, is required for structural integrity and function of synaptic active zones in Drosophila. Neuron *49*, 833-844.

Wang, J.-W., Beck, E.S., and McCabe, B.D. (2012). A modular toolset for recombination transgenesis and neurogenetic analysis of Drosophila. PLoS ONE *7*, e42102.

Wu, Y., Cao, G., Pavlicek, B., Luo, X., and Nitabach, M.N. (2008). Phase coupling of a circadian neuropeptide with rest/activity rhythms detected using a membrane-tethered spider toxin. PLoS Biol *6*, e273.

Yeh, E., Gustafson, K., and Boulianne, G.L. (1995). Green fluorescent protein as a vital marker and reporter of gene expression in Drosophila. Proc Natl Acad Sci USA *92*, 7036-7040.